A value-of-information-based optimal sensor placement design framework for cost-effective structural health monitoring (with application to miter gate monitoring)

Mayank Chadha[1]*, Zhen Hu[2]* , Charles R. Farrar[3] and Michael D. Todd[1]

Abstract

Structural health monitoring (SHM) involves collecting information to assess the health of a structure, typically to guide risk-informed maintenance decision-making or predict limit state behavior throughout its lifespan. Although the value of information (VoI) obtained from an SHM system can facilitate improved decision-making, it is important to estimate its overall utility by considering the costs involved in designing, developing, installing, maintaining, and operating the system. A feasible SHM system provides greater expected returns resulting from data-informed lifecycle management decisions than the cost of the SHM system design, fabrication, deployment, operation, and maintenance. That is, since data acquisition is a precursor to data-informed decision-making, the design of an SHM system governs its feasibility. Such cost-benefit analyses are a current topic of research in the SHM community. One approach that has been proposed for these analyses is a preposterior decision analysis using the VoI metric. In this paper, we propose a sensor optimization framework that maximizes the VoI over the structure's lifecycle, constrained by a pre-decided maintenance policy. We use two different VoI metrics: the traditional expected VoI and a gambling-theory-inspired normalized expected-savings-to-investmentrisk ratio. We introduce three time-normalized, unitless VoI metrics that are valuable for evaluating the performance of an SHM design over an extended period. Furthermore, we consider the effect of different risk profiles on the overall optimal sensor design, recognizing that the cost of decision-making depends on the utility and risk perception of the decision-maker. We conduct a detailed analysis on the marginal utility gain of gathered information as we add more sensors, observing the utility to diminish in line with the law of diminishing returns as the information content increases. This framework is applied to the design of an SHM system used for monitoring miter gates.

Keywords

optimal sensor design, value of information, expected utility theory, Bayesian inference, uncertainty quantification, Bayesian optimization, miter gates

Introduction

Structural health monitoring (SHM) systems aim to detect, localize, and/or quantify damage in a structure and provide engineers with relevant information to make informed choices about maintenance and repairs.[1] Collecting data from an SHM system is valuable as it provides information for making informed decisions and improves our understanding of the system. In other words, the infrastructure required for information acquisition over a period of time comes at a cost.[2–7] Therefore, it is crucial to take into account

the expenses associated with designing, developing, installing, maintaining, and operating the SHM

[1]University of California San Diego, La Jolla CA, USA
[2]University of Michigan Dearborn, Dearborn, MI, USA
[3]Los Alamos National Lab, Los Alamos, NM, USA

*These authors contributed equally.

Corresponding author:
Michael D. Todd, University of California San Diego, 9500 Gilman Drive, Mail Code 0085, La Jolla CA 92093-0085, USA.
Email: mdtodd@ucsd.edu

system. It is essential to use a well-designed SHM system that utilizes an optimized sensing data stream tailored to achieve a specific objective function or utility.

The optimal design of sensors has garnered significant interest in the SHM community. With each application being unique and focusing on specific targets, a wide range of objective functions and solution strategies have been proposed in numerous influential studies within this research field. Within this research field, one group of optimality criteria focuses on sensor design to maximize information gain and minimize uncertainty regarding the structural state. In this context, several commonly used information-based metrics have been introduced. The Fisher information matrix and its variants, such as the trace (referred to as the A-optimality criterion), the determinant (known as the D-optimality criterion), and the largest eigenvalue (referred to as the E-optimality criterion), are employed as information-based metrics in sensor design.[8–13] Another metric that is commonly used to quantify information gain is *f*-divergence, with Kullback–Leibler (KL) divergence being the most popular example. KL divergence measures information gain using relative entropy and has been applied to sensor optimization.[14,15] Probability of detection is another useful metric for sensor optimization. This objective aims to minimize false alarms in detection (type I error) and false negatives in detection (type II error).[16–19] Others have used structural dynamic-specific criteria such as the modal assurance criterion, which quantifies the similarity in mode shapes, in sensor optimization.[20–23] Yang et al.[24] tackled a practical issue of considering the possibility of sensors malfunctioning and used a reliability-based optimality criterion for sensor optimization.

In this paper, we target the feasibility of an SHM system. To determine the viability and long-term sustainability of an SHM program as a life cycle investment, it is essential to assess whether the anticipated expected returns as a result of SHM-system-guided data-informed decision-making will exceed the overall investment in an SHM system throughout the structure's lifespan. This paper aims to provide a fundamental mechanism, through which a structural owner could decide whether investment in a performance-quantified SHM design provides sufficient return on that investment.

This research builds upon our previous work investigating and developing an optimal sensor design solutions for applications in SHM. In a prior publication by Yang et al.,[25] we presented a mathematical and numerical framework for implementing Bayesian optimization in order to achieve optimal sensor design for SHM purposes. In a subsequent publication by Yang et al.,[14] we applied and expanded upon this framework to a real-world case study involving the SHM of a miter gate, which is a component of a lock system used for navigation on inland waterways. Our objective in this case study was to identify a sensor array design that maximized the gain in information, as measured by a class of divergence functions known as *f*-divergence. It should be noted that while information gain is important, it may not always result in an economically optimal design, since the cost of obtaining that information was ignored. Recognizing that the information gathered by an SHM system influences the cost-effectiveness of the decisions it informs (subject to constraint on the maintenance and repair policy adopted by the owners of the structure), our aim is to expand the optimization framework we have built in Refs. 14, 25 and 26 to design an SHM system that maximizes the relative cost benefit of data-informed decision-making in relation to the investment cost. We strive to achieve the optimal balance where the benefits of obtaining and utilizing SHM data outweigh the associated costs, resulting in an economically viable and sustainable SHM program. Such cost-benefit analysis has previously been performed through pre-posterior decision analysis using the value of information (VoI) metric. The excellent contributions by Malings and Pozzi[27,28] emphasized the benefits of using VoI as a metric for optimal sensor placement that supports decision-making, despite the computational complexity involved in evaluating it.

Therefore, this paper's main contributions and originality can be summarized as follows:

1. *Optimal sensor placement design using VoI as the objective function*: This paper adopts a pre-posterior optimization approach that leads to a sensor network design maximizing the VoI metric. For pre-posterior design, no sensor data are available. This sensor design is obtained by simulating the lifecycle of the structure based on reasonable assumptions and uncertainty bounds in sensor data and loading that the structure is subjected to, and by considering a predefined maintenance policy (automated in our case using expected utility theory). Such an investigation is carried out to determine if investing in an SHM system is worthwhile and, if so, what the initial design of an SHM system (with sensor placement design being a small part of it) should be to make it a viable investment. This design methodology represents a crucial step toward creating an SHM program and building an asset management digital twin or cybermodel[29–31] that can provide significant benefits to lifecycle asset management while remaining cost-effective throughout the structure's entire lifespan.

2. *Investigating the impact of different VoI metrics on sensor design*: This paper analyzes the impact of two distinct VoI metrics on SHM system design:

the traditional expected VoI[2,4] and a gambling-theory-inspired normalized expected return-to-investment-risk ratio proposed by Chadha et al.[5]

3. *Proposing three different time-normalized, unitless VoI metrics*: This paper proposes three additional VoI metrics—the arithmetic, geometric, and exponential annual rate of expected savings—that are unitless and time-normalized. These metrics could be beneficial when analyzing the benefits of an information-gathering system over a long time span as a business case.

4. *Investigating the impact of spectrum of utilities and risk profiles on optimal sensor design*: Since decision-makers are the typical curators of SHM utility, this paper also investigates the effect of different risk profiles on the overall optimal sensor design.[32–35]

5. *Sensor placement considering various uncertainties*: The proposed optimal sensor design framework considers various prior information and uncertainties in modeling loading, sensor noise, the cost of maintaining and operating an SHM system over time, and in forecasting damage degradation over the entire lifecycle of the structure while performing the pre-posterior analysis.

6. *Expanding on the previously proposed Bayesian optimization framework*: This paper exploits the optimization framework we built in Refs. 14, 25 and 26 to address the computational challenges inherent in designing a sensor network. These objectives and novelties are achieved through the integration of Bayesian optimization, surrogate modeling, and Bayesian inference using particle filtering techniques. The complexity of the problem, coupled with the need to consider numerous sources of uncertainty (which are multivariate in nature) during the design phase, results in the VoI metric becoming a higher-dimensional integral with a nonlinear integrand. We employ sampling-based Monte Carlo simulation to approximate the expectations in VoI.

7. *Case study on the miter gate structure*: This study showcases the effectiveness of the newly proposed sensor placement design framework on a practical and complex miter gate monitoring application.[36,37] The miter gate structure is an ideal demonstration example for two main reasons. First, the damage parameter in this case is the loss of boundary contact or "gap" between the miter gate and the quoin block at the bottom of the gate, which can be characterized by a one-dimensional continuous state parameter inferred from sensor measurements. Despite being a complex real-world structure, the miter gate's one-dimensional state parameter allows for a more straightforward

analysis. Other failure modes could be considered, but to evaluate new VoI metrics and the subsequent optimization of sensor networks, focusing on a single failure mode is sufficient.

The second reason why the miter gate structure is a suitable example is that the pre-posterior VoI-based sensor optimization requires simulating the lifecycle using a physics-based finite-element model (FEM) and its surrogate, while also considering a maintenance policy that guides the decision-making process for which the sensors need to be optimized. In this study, we were able to use the same FEM model from our previous work[14] and a maintenance policy proposed in Ref. 32 to simplify the process. While we rely on some results from our previous research, we provide a comprehensive explanation of the necessary concepts for this study for completeness. Where required, we also direct readers to the aforementioned papers for further information.

As mentioned earlier, building a sensor design framework depends on the particular application and objective function. In this instance, we aim to utilize the VoI as the objective function to achieve the optimal sensor design for monitoring the miter gate structure. The definition of the VoI metric is reliant on the cost model, maintenance policy, noise model, loading model, damage degradation model, and other aspects that are specific to the structure being monitored. Therefore, we believe that the best way to illustrate the framework is by demonstrating its implementation in a case study focused on the SHM of a miter gate. The remainder of this paper is organized as follows: section "The structure of interest" provides an overview of the miter gate structure and its modeling. Section "The maintenance policy and the cost model" presents a summary of the maintenance policy and cost model adopted in this paper. Section "The VoI metric" presents the VoI metrics used as the objective function for sensor optimization. Section "Optimization and results" describes the Bayesian optimization technique used to solve the optimization problem. It showcases and evaluates the performance of various optimal sensor designs obtained using VoI-based and information-based metrics. Lastly, section "Summary and conclusions" summarizes and concludes this paper.

The structure of interest

Miter gate and the damage parameter

The miter gate is a vital component of the lock system used for inland waterway navigation, which is managed and maintained by the US Army Corps of Engineers (USACE) in the USA. This infrastructure is critical for
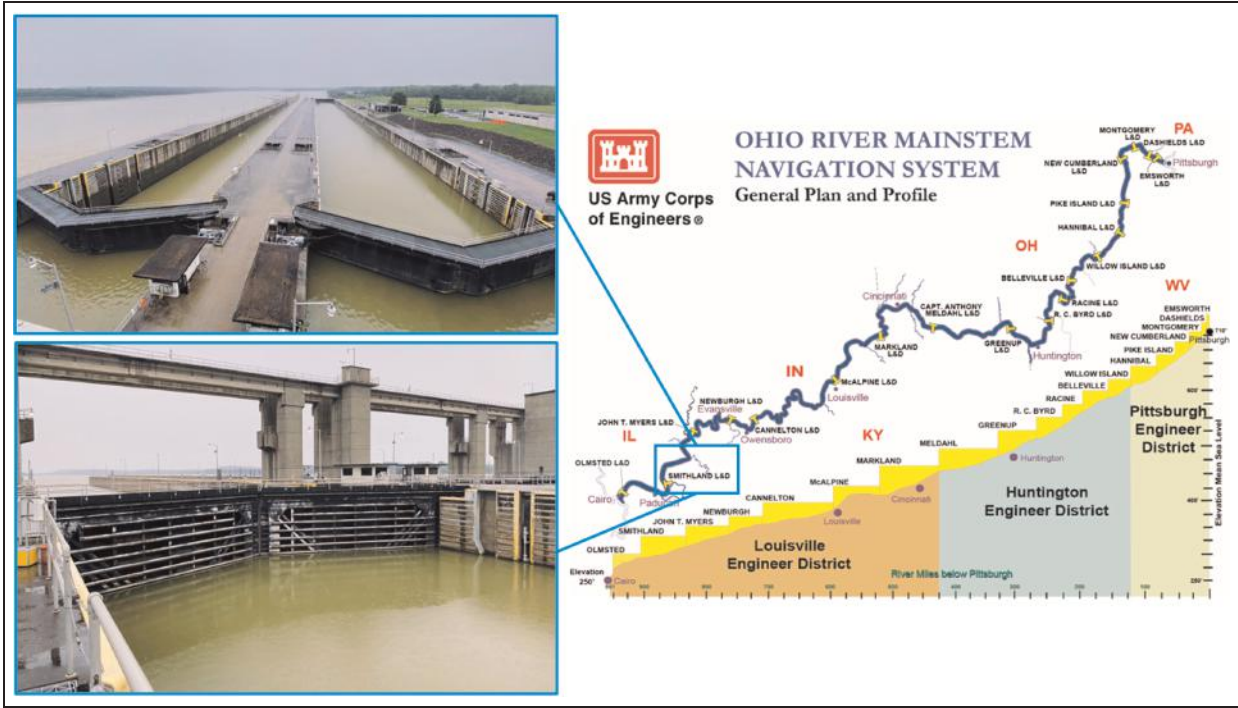
Figure 1. Smithland lock and dam and the general profile of Ohio river navigation system.
Source: Photo credit: Mayank Chadha.

transporting goods through the country's inland river network and is a matter of national economic security. Typically situated in areas with varying water levels, locks consist of a chamber with gates to control the water flow. The miter gate is composed of two hinged panels that meet at an angle (the "miter") when closed, forming a tight seal to prevent water from passing through. When a vessel approaches, the panels are opened to enable safe passage through the lock chamber. The gates at each end of the lock chamber can be closed to create a watertight seal, allowing the water to be raised or lowered as needed. Once the water level in the chamber matches the next section of the river, the gates on that end are opened, allowing the vessel to proceed. In this way, the lock and gate system creates a series of steps that enable boats and ships to navigate through rivers with varying water levels. An example of a lock system managed by USACE is illustrated in Figure 1.

In this paper, we use the Greenup miter gate at the USACE Huntington Engineer District as a case study for simulating the optimal sensor placement design. The gate opens and closes regularly, which results in the gate losing contact with the wall quoin blocks at the bottom of the gate (refer to Figure 4 in Eick et al.[38]). This damage to the boundary is a time-dependent scalar quantity and is referred to as the "gap

length" or simply "gap" and denoted by $\theta(t) \in \Omega_{\Theta(t)}$. For each time instance, we model the gap value as a random variable $\Theta(t)$, where $\theta(t)$ represents a realization of the gap value, and $\Omega_{\Theta(t)}$ denotes the space of gap values. At $\theta = \theta_{\min} = 0$ inches, the gate is pristine. Based on the suggestions from USACE field engineers, the limit $\theta = \theta_{\max} = 180$ inches is assigned as the upper bound of gap length at which point the gate is considered to be nonoperational.

Since the time evolution of the gap length is not precisely known, we model it probabilistically, as shown in Figure 2. For the purpose of illustration, we assume the first 5-year period of the structure as the lifespan of interest, such that the mean value of the prior-gap degradation curve reaches the upper threshold of $\theta_{\max}$ in 5 years. It is important to make this assumption about the lifespan since we are in the pre-posterior stage of design. The applicability of the presented formulation is independent of the lifecycle duration and the chosen degradation model, although the sensor placement results will vary if a different gap degradation curve is chosen. The proposed formulation can easily be adapted to consider a much longer lifecycle without deviating from the proposed methods. The prior distribution of gap length at time t is denoted by $f_{\Theta(t)}(\theta(t))$. The gap evolution over time is described by a piecewise
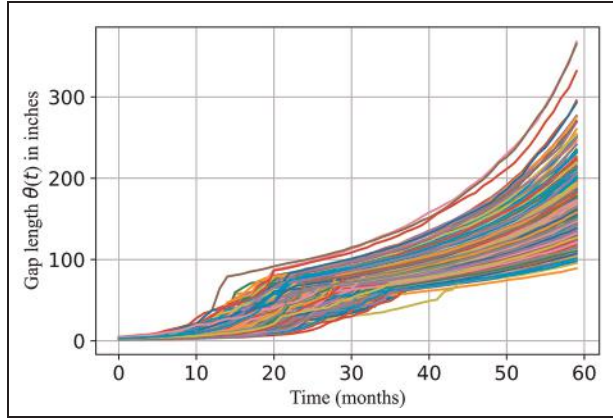
Figure 2. Prior gap-degradation model that probabilistically models time evolution of the gap.

multistage degradation model, which is discussed in section 5.1 of Chadha et al.[5]

The load vector

The gate is subjected to uncertain upstream and downstream hydrostatic loads. We model the upstream and downstream hydrostatic heads as random variables $H_{up}(t)$ and $H_{down}(t)$, respectively, with their respective realizations denoted by h_{up} and h_{down}. Together, we model the load vector, which consists of the upstream and downstream hydrostatic loads, as the random vector $\boldsymbol{H}(t)$, with a realization denoted by $\boldsymbol{h}(t) = (h_{up}(t), h_{down}(t))$. Let $\Omega_{H_{up}(t)}$, $\Omega_{H_{down}(t)}$, and $\Omega_{\boldsymbol{H}(t)}$ denote the space of load vector, upstream water head, and downstream water head, respectively, such that $\Omega_{\boldsymbol{H}(t)} = \Omega_{H_{up}(t)} \times \Omega_{H_{down}(t)}$.

The water heads over the lifespan of the miter gate are probabilistically modeled by time-series models using autoregressive moving average (ARMA) as follows:

$$\begin{aligned}
h_{up}(t_i) &= 172 + \varepsilon_i^{up} + 0.33 h_{up}(t_{i-1}) + 0.35 h_{up}(t_{i-2}) \\
&\quad + 0.52 \varepsilon_{i-2}^{up} + 0.55 \varepsilon_{i-1}^{up}, \quad \text{where,} \quad \varepsilon_i^{up} \sim N(0, 2^2); \\
h_{down}(t_i) &= 95 + \varepsilon_i^{down} + 0.23 h_{down}(t_{i-1}) + 0.25 h_{down}(t_{i-2}) \\
&\quad + 0.52 \varepsilon_{i-2}^{down} + 0.61 \varepsilon_{i-1}^{down}, \quad \text{where,} \quad \varepsilon_i^{down} \sim N(0, 2^2).
\end{aligned}$$
(1)

Here, ε_i^{up} and ε_i^{down} represent errors in the upstream and downstream height at time step i, respectively, and are assumed to be modeled by a normal distribution with a zero mean and variance within an acceptable range. Figure 3 illustrates one realization of the hydrostatic head time series constructed using ARMA over a 60-month time period.

Simulating the observed sensor measurements using an FEM and its surrogate

The submerged part of the gate that loses contact is difficult to directly measure due to highly turbid water. Therefore, the gap length needs to be inferred from indirect measurements. We simulate our data acquisition process using a high-fidelity FEM of the Greenup miter gate previously validated in the undamaged condition with the available strain sensor readings. Although there are infinitely possible locations where strain gauges can be placed on a real miter gate, the FEM discretely covers the countable number of sensor locations by calculating strain values at the integration points that we choose as strain measurement locations. As demonstrated in Fig. 3 of Chadha et al.,[5] the FEM itself is constructed using 3D quadrilateral and triangular shell elements in ABAQUS and consists of a total of 64,919 elements. Each element is identified by its
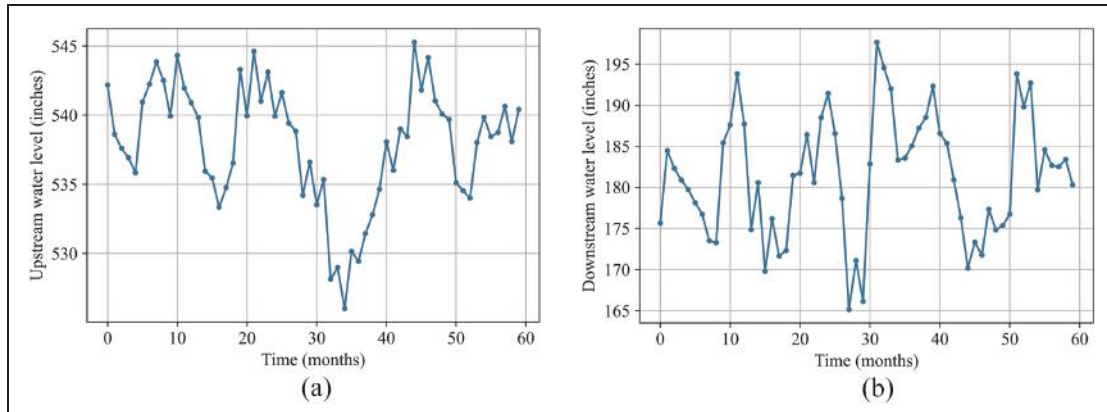
Figure 3. Realization of the hydrostatic water head time series: (a) upstream water level and (b) downstream water level.

geometric centroid at the origin of the local coordinate system. For each element, there are four possible *simulated strain gauge* locations. Strain values from the FEM model can be obtained both horizontally and vertically on both the top and bottom surfaces of the element. These four combinations are denoted by TH, TV, BH, and BV, where T stands for top surface of an element, B stands for bottom surface of an element, H stands for horizontal orientation, and V stands for vertical orientation (see section 4.1 of Chadha et al.[5] for more details). Therefore, in total, there are $64,919 \times 4$ sensor locations of choice. However, for practical reasons, the USACE installs the sensors only on the downstream side of the miter gate. This reduces our available sensor locations by approximately half. We denote the number of all possible sensor locations as $N_{\text{Total−Sensors}}$, and for the chosen miter gate case study, it is $64,919 \times 2$.

Given a specific value of gap length and hydrostatic heads, denoted by $(\theta(t), h_{\text{up}}(t), h_{\text{down}}(t))$, both the FEM and its digital surrogate simulate the "true" strain values (without noise) for all $N_{\text{Total−Sensors}}$ sensors (i.e., we assume the FEM model to be the ground truth). The process of Bayesian optimization requires numerous realizations of the "true" strain values. The digital surrogate of FEM, denoted by $g(\theta(t), h_{\text{up}}(t), h_{\text{down}}(t))$, is created to speed up the simulation process. To create the digital surrogate, we utilize Gaussian process regression (GPR) in conjunction with single value decomposition. For more information on the FEM and digital twin, refer to sections 2.1 and 2.2 of Yang et al.[14] As such, we model the simulated observed strain measurements by the random vector X, which consists of $N_{\text{Total−Sensors}}$ simulated strain measurements (each modeled as a random variable X_i). The observed strain measurements consist of two additive components: the first is the "true" strain values obtained using the digital twin of the FEM model, and the second is the measurement noise. The noise is modeled as a random vector ζ with a realization $\varepsilon \in \Omega_z$. Here, Ω_z denotes the space of noise vector. We assume that e follows a zero-mean Gaussian distribution with independent components. In other words, the noise terms of different strain gauges are statistically independent, and the noise in the i-th strain gauge is modeled as $\varepsilon_i \sim N(0, \sigma_{\varepsilon_i}^2)$. Furthermore, we assume that each strain gauge has the same standard deviation, and the standard deviation of noise is assigned to be $\sigma_{\varepsilon_i} = 5 \times 10^{-6}$ in accordance with reasonable commercial strain gauge performance. We note that another alternative approach for assuming strain gauge measurement uncertainty could be utilizing the observed characteristics of the sensors installed on-site, if available (such as those used to calibrate the FEM model). In some cases, this might be a more realistic representation of measurement uncertainties since sensor performance also depends on the quality of implementation in addition to their intrinsic manufactured characteristics. The strain measurements model is given as:

$$x = g(\theta(t), h_{\text{up}}(t), h_{\text{down}}(t)) + \varepsilon. \quad (2)$$

Let Ω_E denote the exhaustive design space consisting of all the possible designs. For $N_{\text{Total−Sensors}} = 64,919 \times 2$, the total number of possible designs is given by:

$$\text{length}(\Omega_E) = \sum_{r=1}^{N_{\text{Total−Sensors}}} \frac{N_{\text{Total−Sensors}}!}{r!(N_{\text{Total−Sensors}} − r)!} \quad (3)$$
$$= (2^{N_{\text{Total−Sensors}}} − 1) \approx 10^{39,085}.$$

Consider an instance e of a design belonging to the set Ω_E. The design e consists of $N_{\text{sg}}(e)$ sensors. Let $x_e = (x_{e1}, x_{e2}, \ldots, x_{eN_{\text{sg}(e)}}) \in \Omega_{X_e} \subset \Omega_X$ denote a realization of the random vector X_e that models the "observed" strain measurements corresponding to the sensors in the design e. The measurement model for the strain gauges included in the design e is given by:

$$x_e = g_e(\theta(t), h_{\text{up}}(t), h_{\text{down}}(t)) + \varepsilon_e. \quad (4)$$

Here, $g_e(\theta(t), h_{\text{up}}(t), h_{\text{down}}(t)) = (g_{e1}, g_{e2}, \ldots, g_{eN_{\text{sg}(e)}})$ is the simulated "true" strain values of gauges in design e obtained using the digital surrogate of the FEM. The vector $\varepsilon_e = (\varepsilon_{e1}, \varepsilon_{e2}, \ldots, \varepsilon_{eN_{\text{sg}(e)}}) \in \Omega_{z_e} \subset \Omega_z$ represents the measurement noise vector for the design e.

Using the measurement model defined in Equation (4), the likelihood of observing the strain measurement $x_e \in \Omega_{X_e}$ for the gap length $\theta(t)$ can be written as:

$$f_{X_e|\Theta}(x_e|\theta) = \prod_{i=1}^{N_{\text{sg}}(e)} \frac{1}{\sigma_{\varepsilon_{ei}}} \phi\left(\frac{x_{ei} − g_{ei}(\theta(t), h_{\text{up}}(t), h_{\text{down}}(t))}{\sigma_{\varepsilon_{ei}}}\right).$$
$$(5)$$

The relationship between gap length and strain data is highly nonlinear and complex. As a result, we use particle filters to numerically infer the posterior distribution. This process is detailed in section 2.4 of Ref. 14.

The maintenance policy and the cost model

The binary maintenance policy

The USACE considers an operational conditional assessment rating protocol for its miter gate structures. This protocol consists of six discrete damage labels: A (excellent), B (good), C (fair), D (poor), F (failing), and CF (complete failure). These ratings generally reflect the increased overall damage state.[39] In contrast to the nonbinary rating protocol used by USACE, in our study (Chadha et al.[32]), we proposed a simplified

binary labeling system for the miter gate. This rating system has two discrete damage labels, resulting in a binary decision space denoted as $\Omega_D = \{d_0, d_1\}$. These labels are defined as follows:

d_0: label indicating that the gate is undamaged with excellent operational capacity;

d_1: label indicating that the gate is damaged and is not safely operational. $\qquad$ (6)

Let M_0 and M_1 represent the actions associated with the labels d_0 and d_1 respectively, such that

M_0: Continue regular operation;

M_1: Shutdown, inspect, and repair or replace as required based on the inspection results. $\quad$ (7)

In the way this problem is posed, the labels d_i have a one-to-one correspondence with the maintenance actions M_i. This may seem redundant; however, our intention here is to define a bijective relationship between the *discrete damage labels* and the *maintenance actions* warranted for the structure. For example, in the way the decision space is defined, if the structure is undamaged, then no maintenance is warranted. Conversely, if maintenance is not a recommended action, it means the structure is undamaged. As a consequence, choosing the decision space to be defined by the set $\{d_0, d_1\}$ is equivalent to choosing the decision set $\{M_0, M_1\}$.

We consider four different costs in the evaluation of the VoI, which are listed below:

1. Cost A: Inflation-adjusted, utility-adjusted consequence cost of performing a maintenance action on the structure.
2. Cost B: Maintenance cost of an SHM system over time adjusted for inflation
3. Cost C: Operation cost of an SHM system over time adjusted for inflation
4. Cost D: Cost of design and initial installation of an SHM system incurred one time at the beginning

In the following subsections, we elaborate on the various cost models used for VoI analysis and subsequently for sensor optimization in this paper.

The base cost model

For this paper, we have chosen to utilize the maintenance policy and cost structure proposed in Chadha et al.[32] to evaluate our sensor designs. It should be noted that we can readily apply any other maintenance policy and obtain sensor designs using the framework presented in this paper.
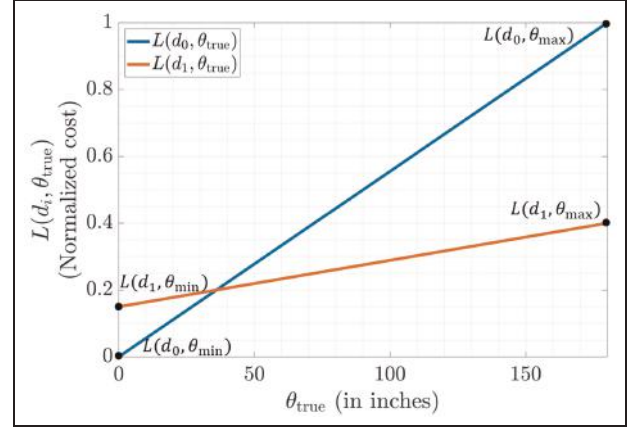
Figure 4. Assumed linear base consequence cost (normalized) for decision scenario d_0 and d_1.

Let $L(d_0, \theta_{\text{true}})$ and $L(d_1, \theta_{\text{true}})$ denote the consequence costs of performing the maintenance actions M_0 and M_1, respectively, when the true degree of damage is defined by θ_{true}, such that:

$$L(d_0, \theta_{\text{true}}) = \left(\frac{L(d_0, \theta_{\max}) - L(d_0, \theta_{\min})}{\theta_{\max} - \theta_{\min}} \right) \theta_{\text{true}} + L(d_0, \theta_{\min});$$

$$L(d_1, \theta_{\text{true}}) = \left(\frac{L(d_1, \theta_{\max}) - L(d_1, \theta_{\min})}{\theta_{\max} - \theta_{\min}} \right) \theta_{\text{true}} + L(d_1, \theta_{\min}).$$

$$(8)$$

In the equation above, the extremes costs $L(d_i, \theta_{\min})$ and $L(d_i, \theta_{\max})$ are assumed to be known and estimated by the organization. Because $L(d_0, \theta_{\max})$ is the maximum extreme cost, all other extreme costs can be expressed as a fraction of $L(d_0, \theta_{\max})$. For the purposes of numerical simulation, we assume $L(d_1, \theta_{\min}) = 0.15 L(d_0, \theta_{\max})$ and $L(d_1, \theta_{\max}) = 0.4 L(d_0, \theta_{\max})$. We assign a normalized cost value of 1 unit to $L(d_0, \theta_{\max})$.

The consequence costs of performing maintenance M_0 and M_1, denoted by $L(d_0, \theta_{\text{true}})$ and $L(d_1, \theta_{\text{true}})$, as illustrated in Fig. 4, are assumed to have linear profiles. Readers are referred to section 4.2 of Chadha et al.[32] for the detailed rationale behind this assumption. We carefully note that the functional form of this consequence function need not necessarily be linear and may vary depending on the problem, target objective, damage type, or the definition and nature of the limit state (e.g., which can be continuous or discrete), and the sheer complexity of the problem.

For instance, consider the decision scenario d_0. The current linear functional form of $L(d_0, \theta_{\text{true}})$ assumes that the consequence of choosing d_0 increases linearly with the increase in damage levels over time. That is, θ_{true} increases over time, and so does the consequence cost $L(d_0, \theta_{\text{true}})$. Additionally, based on the assumed
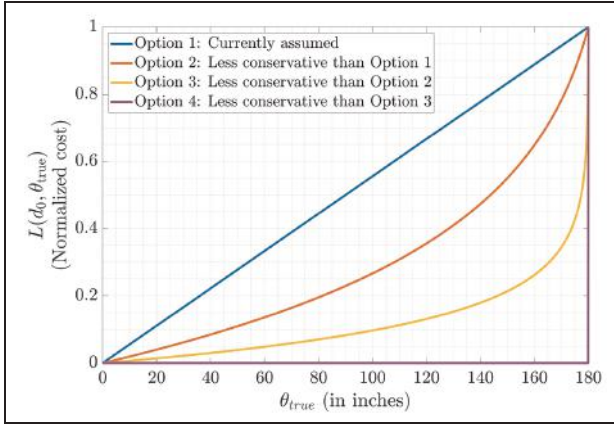
Figure 5. Some possible functional forms of the base consequence cost curves $L(d_0, \theta_{\text{true}})$.

prior gap degradation model illustrated in Figure 2, θ_{true} will be one of the realizations of the distribution $f_{\Theta(t)}(\theta(t))$. Therefore, the consequence cost needs to be distributed over the damage space since it is hard to pinpoint the exact value of θ_{true} at the end of the assumed lifecycle. For example, based on the assumed prior gap evolution model, as shown in Figure 2, at the end of the assumed lifecycle, θ_{true} can be anywhere between $[90, 380]$ inches.

Based on this discussion, it is clear that the consequence of making decision d_0 approaches a false-positive case as damage increases over time and a logical functional form must capture this trend. The assumed linear functional form of $L(d_0, \theta_{\text{true}})$ provides two advantages: (a) it is a simple and logical function, and (b) it is a desirably conservative consequence function. Alternatively, one can assume less conservative yet reasonable functional forms, recognizing that the danger of decision d_0 leading to the worst-case false-positive decision *accelerates* as the damage level approaches the assumed threshold. Figure 5 shows three other alternative functional forms of $L(d_0, \theta_{\text{true}})$:

The utility model and utility-adjusted consequence cost

In making maintenance decisions based on an organization's policies or collective experience, we must consider the real-world scenario in which inspection engineers execute these decisions. However, because these decisions are subjective to the engineer's experience and thought processes, there may be slight differences in cost consequences compared to the base cost function. To account for the decision-maker's risk profile, we can use a mathematical model that incorporates their utility function. The utility function represents how an individual evaluates the outcome of an action,

which may differ from its real dollar cost. A risk-averse decision-maker will assign a higher value to cost/loss than its real dollar cost, resulting in a concave-down utility function. On the other hand, a risk-seeking decision-maker will assign a lower value to cost/loss, resulting in a concave-up utility function. Chadha et al.[32] discuss how to use an individual's utility function to obtain modified cost functions that incorporate their risk perception into the decision-making process. These risk-adjusted cost functions are denoted by a hat symbol $(\hat{\cdot})$ and are expressed as:

$$
\begin{aligned}
\hat{L}(d_0, \theta_{\text{true}}; \gamma, \xi) &= a_0 \\
&\log\left(1 + b_0\left(\frac{L(d_0, \theta_{\max}) - L(d_0, \theta_{\min})}{\theta_{\max} - \theta_{\min}}\right)\theta_{\text{true}}\right) \\
&+ L(d_0, \theta_{\min}); \\
\hat{L}(d_1, \theta_{\text{true}}; \gamma, \xi) &= a_1 \\
&\log\left(1 + b_1\left(\frac{L(d_1, \theta_{\max}) - L(d_1, \theta_{\min})}{\theta_{\max} - \theta_{\min}}\right)\theta_{\text{true}}\right) \\
&+ L(d_1, \theta_{\min}).
\end{aligned}
\tag{9}
$$

The parameters (γ, ξ) defines the risk profile. For a given profile, the constants a_0, a_1, b_0, and b_1 can be obtained by solving Equations (18) and (19) in Chadha et al.[32] It is worth noting that the following conditions define the characteristics of the risk profile:

$$
\begin{aligned}
&\hat{L}(d_i, \theta_{\text{true}}; \gamma, \xi) > L(d_i, \theta_{\text{true}}) \text{ or } \xi < \gamma: \\
&\quad \text{for risk} - \text{averse profile}; \\
&\hat{L}(d_i, \theta_{\text{true}}; \gamma, \xi) = L(d_i, \theta_{\text{true}}) \text{ or } \xi = \gamma: \\
&\quad \text{for risk} - \text{neutral profile}; \\
&\hat{L}(d_i, \theta_{\text{true}}; \gamma, \xi) < L(d_i, \theta_{\text{true}}) \text{ or } \xi > \gamma: \\
&\quad \text{for risk} - \text{seeker profile}.
\end{aligned}
\tag{10}
$$

One of the key conclusions in Chadha et al.[5] was: "As the intensity of risk-aversion behavior increases, the flexibility to choose a feasible SHM system decreases. This is because a risk-averse decision-maker makes more conservative and expensive decisions. For an SHM system to be feasible in the scenario where maintenance decisions are expensive, it must cost less." Therefore, it is of interest to consider the impact of behavioral biases in the optimal sensor placement. For that, we consider three risk profiles defined in Table 1 and illustrated in Figure 6:

Inflation-adjusted costs

Cost A: inflation-adjusted utility-adjusted consequence cost. Let $r(t)$ denote the assumed future monthly rate of inflation at time t in months. It can either be assumed a constant or a time series that is forcasted

Table 1. Three profiles considered to investigate the impact of behavioral biases on sensor design.

Risk profiles	ID	γ	ξ
Risk averter	RP1	0.8	0.6
Neutral risk bearer	RP2	0.8	0.8
Risk seeker	RP3	0.8	0.95

depending on the past treasuries interest rate, CPI (Consumer Price Index) data, Phillips curve, and other macro variables.[40] The factor $(r(t) + 1)^t$ adjusts for the cost of future inflation. The inflation-adjusted utility-adjusted consequence cost of decision-making is then given by:

$$\hat{\tilde{L}}(d_i, \theta_{\text{true}}, t; \gamma, \xi) = \hat{L}(d_i, \theta_{\text{true}}; \gamma, \xi)(r(t) + 1)^t. \quad (11)$$

The inspection and maintenance decisions are usually carried out at discrete time steps. We assume a

discrete-time space $\Omega_{T_A} = \{t_{A_1}, t_{A_2}, ..., t_{A_{N_A}}\}$ consisting of N_A time steps. Figures 7 and 8 illustrate how the inflation-adjusted utility-adjusted consequence costs evolve over time for different values of a constant annual inflation rate. We note that the impact on cost escalation becomes markedly more pronounced with higher inflation rates, especially over extended periods. The compounding effect of inflation causes costs to rise exponentially rather than linearly, resulting in a significant disparity between low and high inflation scenarios as time progresses, as observed in Figures 7 and 8.

Consequently, higher inflation rates lead to a substantially greater increase in future costs, underscoring the importance of accounting for inflation in long-term cost planning and decision-making. In this paper, we assume a fixed inflation rate of $r(t) = 2\%$.

Cost B and Cost C: inflation-adjusted maintenance and operation cost of the SHM system. Let the inflation adjusted
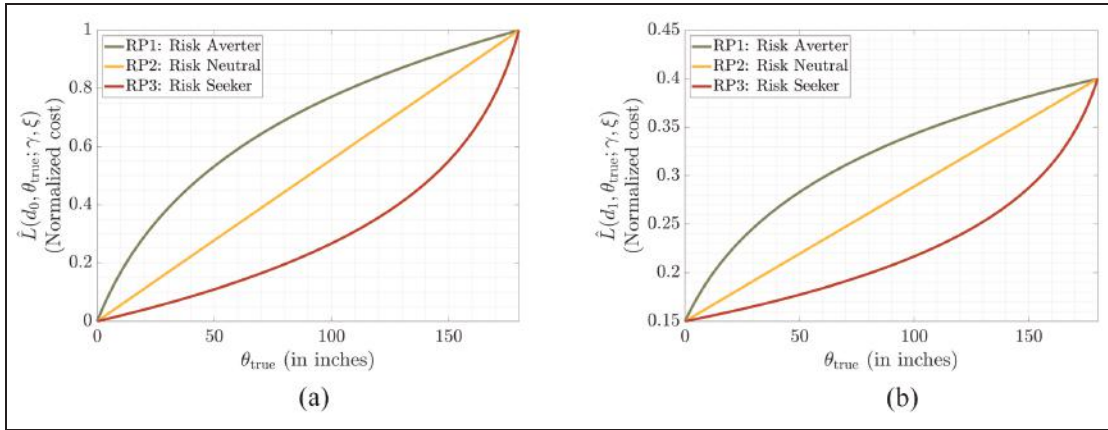
Figure 6. Utility-adjusted consequence cost of decision-making: (a) for decision scenario d_0 and (b) for decision scenario d_1.
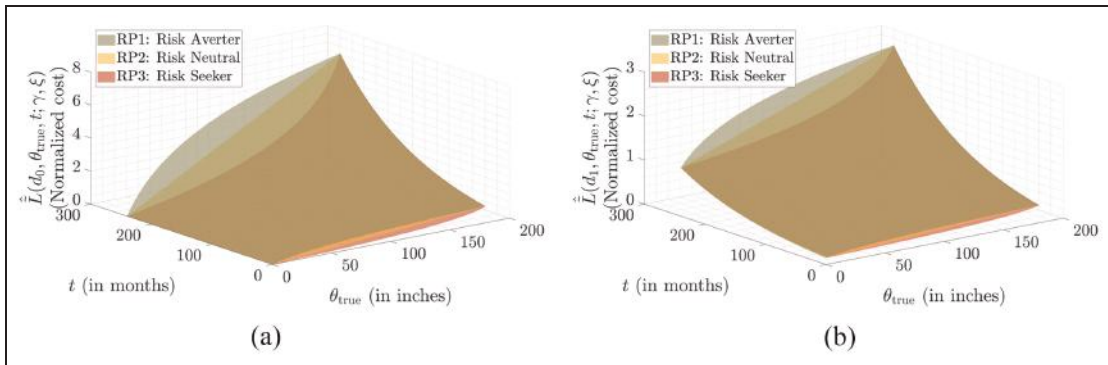
Figure 7. Inflation-adjusted utility-adjusted consequence cost considering a constant annual inflation rate of 2%: (a) for decision scenario d_0 and (b) for decision scenario d_1.
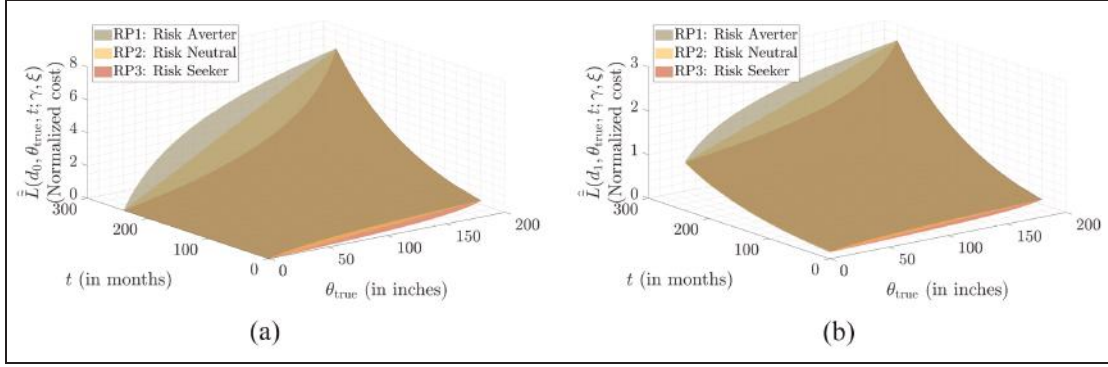
Figure 8. Inflation-adjusted utility adjusted consequence cost considering a constant annual inflation rate of 10%: (a) for decision scenario d_0 and (b) for decision scenario d_1.

maintenance and operation cost be denoted by $C_M(t)$ and $C_O(t)$ defined as:

$$C_M(t) = C_M(r(t)+1)^t;$$
$$C_O(t) = C_O(r(t)+1)^t. \tag{12}$$

Here, C_M denotes the current estimated cost for one instance of maintenance of the system, and C_O denotes the currently estimated operation cost per month. Assuming that the maintenance is done periodically, we define the discrete time space for maintenance as $\Omega_{T_B} = \{t_{B_1}, t_{B_2}, \ldots, t_{B_{N_B}}\}$, containing N_B time steps (not necessarily uniform). Similarly, we assume that the operational cost is evaluated every month defined by the discrete time space $\Omega_{T_C} = \{t_{C_1}, t_{C_2}, \ldots, t_{C_{N_C}}\}$ containing N_C time steps (not necessarily uniform). For consistency in calculations, we normalize the maintenance and operations cost by the factor $L(d_0, \theta_{\max})$ that was used to normalize the base consequence cost.

Cost D: cost of design and installation. The cost of designing and initially installing an information gathering system is denoted as $C(e)$, which we assume to be an initial cost and hence time and inflation-independent. For consistency in calculations, we normalize the cost $C(e)$ by the factor $L(d_0, \theta_{\max})$ that was used to normalize the base consequence cost.

The VoI metric

The VoI metric over the structure's lifecycle

To define and evaluate the VoI metric in the *pre-posterior stage*, it is necessary to simulate the decision-making process over the structure's life cycle. We use expected utility theory (EUT) to determine the optimal action, selected from a pre-defined set of decisions or actions, such as the simple set of maintenance actions laid out

in Equation (7), at a given moment based on new information about the structure's health.

When there is no SHM system and no additional information about the system, the probabilistic state of the structure at time t is captured by the prior distribution of the damage parameter, denoted by $f_{\Theta(t)}(\theta(t))$. The optimal decision $d_{\text{prior}}(t)$ is obtained as follows:

$$d_{\text{prior}}(t) = \text{argmin}_{d_i} E_{\Theta(t)}\left[\hat{\tilde{L}}(d_i, \theta(t), t; \gamma, \xi)\right]. \tag{13}$$

Similarly, when new information is available, such as strain readings $x_e(t)$, the updated structural state is represented by the posterior distribution of damage, denoted by $f_{\Theta(t)|X_e(t)}(\theta(t)|x_e(t))$. The optimal decision $d_{\text{posterior}}(x_e(t), t)$ that minimizes the expected consequence cost (or Bayes' risk) is given as follows:

$$d_{\text{posterior}}(x_e(t), t) = \text{argmin}_{d_i} E_{\Theta(t)|X_e(t)}\left[\hat{\tilde{L}}(d_i, \theta(t), t; \gamma, \xi)\right]. \tag{14}$$

Note that these decisions, obtained using EUT, minimize the expected consequence cost. It is expected that, on average, data-informed decisions, or *posterior decision analysis*, will lead to net savings compared to decisions made without any information or *prior decision analysis* (this will be discussed in more detail in Remark 1). Optimal sensor design in the early stage and VoI analysis are both pre-posterior activities. Pre-posterior decision analysis is a framework that helps decision-makers evaluate the potential benefits of gathering additional information without actually installing an information-gathering system. It is assumed that the acquired information is *imperfect* and is subject to uncertainties. In most practical problems, the state parameter is not directly measured; rather, it is inferred from other attainable measurements that inherently have measurement noise.

Performing a posterior decision analysis, which involves selecting a maintenance option from the available choices, requires using the updated state of the structure (i.e., the posterior distribution of the gap) and the associated consequence cost (Cost A) within the EUT framework. Now, let us consider two ways to perform the prior decision analysis. First, we could consider the EUT framework, where prior knowledge of the damage is taken into account (e.g., if we have no prior knowledge of the damage, we could assume the prior distribution of the gap to be a uniform distribution representing lack of knowledge) and evaluate the optimal decision by considering the consequence cost based on the EUT. Alternatively, we could consider how inspections and maintenance were done in the field by the engineers without any SHM system. For example, the engineers could perform scheduled periodic inspections and maintenance repairs. To evaluate the expected cost savings resulting from using an SHM system and making data-informed decisions, we need to compare the maintenance costs incurred in posterior and prior decision analyses. To maintain consistency, we use the EUT-based information-led automated decision model for both posterior and prior decision-making (the former case). By doing so, we ensure that there are net positive savings resulting from data-informed SHM-supported decision-making when the cost of information acquisition is ignored, and the information is representative of the true reality despite the inherent uncertainty in the data acquisition process. *In other words, unbiased and free-of-cost information is always beneficial.*

We use two VoI metrics derived in section 5.3 of Chadha et al.[5] as objective functions to obtain the optimal sensor design. First, we define the *Expected VoI over the lifecycle* as:

$$\text{EVoI}_{\text{LC}}(e; \gamma, \xi) = C_{\text{savedLC}}(e; \gamma, \xi) - C_{\text{investedLC}}(e). \quad (15)$$

Here, $\text{EVoI}_{\text{LC}}(e; \gamma, \xi)$ has the units of normalized cost. Expected VoI over the lifecycle depends on two variables: first the sensor design e that acquires information, and secondly, the risk profile, parameterized by (γ, ξ), used to make decisions. In the equation above, $C_{\text{invested LC}}(e)$ denotes the net investments made in the

SHM system over the structure's lifecycle and is defined as follows:

$$C_{\text{investedLC}}(e) = C(e) + C_{M\&O}(e). \quad (16)$$

We notice that $C_{\text{investedLC}}(e)$ is a positive quantity. Here, $C(e)$ is the initial design and build cost of the SHM system, and $C_{M\&O}(e)$ denotes the total cost of maintenance and operation of the SHM system over the lifespan of the structure. Let C_M denote the current estimated cost of maintenance for one instance of system maintenance, and C_0 denote the current estimated operation cost per month. We assume that the maintenance of the data-gathering system is done at discrete time steps, defined by the set $\{t_{B_i}\}$. Similarly, it is assumed that the operational cost is evaluated every month, defined by the set of discrete time instances $\{t_{C_i}\}$. The cost of maintenance and operations for the SHM system over the structure's lifecycle is given by:

$$C_{M\&O}(e) = \sum_{n=1}^{N_B} C_M \cdot (r(t_{B_n}) + 1)^{t_{B_n}} + \sum_{n=1}^{N_C} C_0 \cdot (r(t_{C_n}) + 1)^{t_{C_n}}. \quad (17)$$

The quantity $C_{\text{savedLC}}(e; \gamma, \xi)$ in Equation (15) denotes the expected savings over the lifecycle of the structure as a consequence of making data-informed decisions depending upon the risk profile parameterized by (γ, ξ). As discussed at the beginning of section "The VoI metric over the structure's lifecycle," we use an automated decision-making procedure that utilizes EUT to select the action which minimizes the expected cost as a consequence of making a decision. Therefore, the expected savings, $C_{\text{savedLC}}(e; \gamma, \xi)$, are obtained by subtracting the expected cost incurred due to data-informed *posterior decision analysis* from the expected cost arising from *prior decision analysis*. Since data-informed decision-making (assuming that the sensors are subjected to measurement noise but no bias) provides a better state estimate and therefore leads to informed decisions, it overall reduces the decision cost in comparison to the case where no data is available. Consequently, by definition, $C_{\text{savedLC}}(e; \gamma, \xi)$ is a positive quantity and is given by:

$$C_{\text{savedLC}}(e; \gamma, \xi) = \overbrace{\sum_{n=1}^{N_A} \left(\min_{d_i} E_{\Theta(t_{A_n})} \left[\hat{\tilde{L}}(d_j, \theta(t_{A_n}), t_{A_n}; \gamma, \xi) \right] \right)}^{\text{Expected cost of prior decision analysis over structure's lifecycle}}$$
$$- \underbrace{\sum_{n=1}^{N_A} \left(E_{X_e(t_{A_n})} \left[\min_{d_i} E_{\Theta(t_{A_n})|X_e(t_{A_n})} \left[\hat{\tilde{L}}(d_j, \theta(t_{A_n}), t_{A_n}; \gamma, \xi) \right] \right] \right)}_{\text{Expected cost of data-informed posterior decision analysis over structure's lifecycle}}. \quad (18)$$

The second VoI metric we use is the risk-adjusted return ratio for lifecycle cost analysis, which is defined as:

$$\lambda_{\mathrm{LC}}(e; \gamma, \xi) = \frac{C_{\mathrm{savedLC}}(e; \gamma, \xi)}{C_{\mathrm{investedLC}}(e)}. \quad (19)$$

An SHM system is feasible over the structure's lifecycle if $\mathrm{EVoI}_{\mathrm{LC}}(e; \gamma, \xi) \geqslant 0$ and $\lambda_{\mathrm{LC}}(e; \gamma, \xi) \geqslant 1$. Although these statements are equivalent in the sense that they both imply a net positive return for an SHM system ($C_{\mathrm{savedLC}}(e; \gamma, \xi) \geqslant C_{\mathrm{investedLC}}(e)$), these metrics have fundamental differences in the way they quantify the VoI.

The $\mathrm{EVoI}_{\mathrm{LC}}(e)$ is a differential metric that measures the difference between expected cost-savings and the investment made over the lifecycle of the structure, yielding net expected savings from using an SHM system. Hence, maximizing $\mathrm{EVoI}_{\mathrm{LC}}(e; \gamma, \xi)$ leads to maximizing *absolute* return on investment, while maximizing $\lambda_{\mathrm{LC}}(e; \gamma, \xi)$ maximizes the *ratio* of expected savings to the investment cost. Second, $\mathrm{EVoI}_{\mathrm{LC}}(e)$ has units in dollars, whereas $\lambda_{\mathrm{LC}}(e; \gamma, \xi)$ is a unitless VoI metric.

Remark 1: We can write $C_{\mathrm{savedLC}}(e; \gamma, \xi)$ as:

$$C_{\mathrm{savedLC}}(e) = \int_{\Omega_T} C_{\mathrm{saved}}(e, t; \gamma, \xi)\mathrm{d}t \approx \sum_{n=1}^{N_A} C_{\mathrm{saved}}(e, t_{A_n}; \gamma, \xi). \quad (20)$$

Here, $C_{\mathrm{saved}}(e, t; \gamma, \xi)$ gives the expected cost saved by virtue of making a data-informed decision at time t. Mathematically:

$$C_{\mathrm{saved}}(e, t; \gamma, \xi) = \min_{d_i} E_{\Theta(t)}\left[\hat{\tilde{L}}\left(d_j, \theta(t), t; \gamma, \xi\right)\right]$$
$$- E_{X_e(t)}\left[\min_{d_i} E_{\Theta(t)|X_e(t)}\left[\hat{\tilde{L}}\left(d_j, \theta(t), t; \gamma, \xi\right)\right]\right]. \quad (21)$$

Equivalently, using the definitions of optimal prior and posterior decisions in Equations (13) and (14), the expression for $C_{\mathrm{saved}}(e, t; \gamma, \xi)$ can be written as:

$$C_{\mathrm{saved}}(e, t; \gamma, \xi) = E_{\Theta(t)}\left[\hat{\tilde{L}}\left(d_{\mathrm{prior}}(t), \theta(t), t; \gamma, \xi\right)\right]$$
$$- E_{X_e(t)}\left[E_{\Theta(t)|X_e(t)}\left[\hat{\tilde{L}}\left(d_{\mathrm{posterior}}(\mathbf{x}_e(t), t), \theta(t), t; \gamma, \xi\right)\right]\right]. \quad (22)$$

Notice that the second term in Equation (21) for calculating $C_{\mathrm{saved}}(e, t; \gamma, \xi)$ involves obtaining an average of the consequence cost not only for the posterior distribution of the gap but also for different values of sensor measurements. This is because we assume that the information is *imperfect* due to noise in sensor measurements. Therefore, $C_{\mathrm{saved}}(e, t; \gamma, \xi)$ calculates the overall benefit of data-informed decision at time t in an *average sense*. The value of $C_{\mathrm{saved}}(e, t; \gamma, \xi)$ is always positive because it quantifies monetary gain as a result of information availability and does not include the cost of the SHM system. In other words, the equation $C_{\mathrm{saved}}(e, t; \gamma, \xi) \geqslant 0$ holds true for any time t and any risk profile (γ, ξ), as long as the design e yields unbiased and reliable measurements. It is of interest to investigate how various sensor designs perform in terms of saving due to data-informed decision-making over time. For this purpose, $C_{\mathrm{saved}}(e, t; \gamma, \xi)$ serves as a good metric, and a particular quantity of interest is the time at which the design e yields maximum savings, denoted by $\tau(e; \gamma, \xi)$, such that:

$$\tau(e; \gamma, \xi) = \underset{t}{\arg\max}\, C_{\mathrm{saved}}(e, t; \gamma, \xi). \quad (23)$$

Remark 2: Solving Equation (21) is computationally challenging for two main reasons: (1) the evaluation of the expectations of consequence function in the presence of uncertainty sources is numerically difficult, and (2) the prior and posterior distributions of the damage parameter are not explicitly known. Considering that we can directly obtain samples of the prior distribution of gap length $f_{\Theta}(t)(\theta(t))$ and the posterior distribution of gap length $f_{\Theta(t)|X_e(t)}(\theta(t)|x_e(t))$ through the multistage degradation model and Bayesian model updating, respectively, in this paper, the value of $C_{\mathrm{savedLC}}(e; \gamma, \xi)$ is estimated using sampling-based Monte Carlo simulation. We generate large number of random samples of $\theta_k(t_{A_n}) \in \Omega_{\Theta(t_{A_n})}$ and $\mathbf{x}_{e_k}(t_{A_n}) \in \Omega_{X_e(t_{A_n})}$, with $k \in \{1, 2, 3, \cdots, N_{\mathrm{mcs}}\}$. Here, N_{mcs} denotes the number of Monte Carlo samples. The value of $C_{\mathrm{savedLC}}(e)$ is then approximated as:

$$C_{\mathrm{savedLC}}(e; \gamma, \xi) \approx \sum_{n=1}^{N_A}\left(\min_{d_i}\frac{1}{N_{\mathrm{mcs}}}\sum_{k=1}^{N_{\mathrm{mcs}}}\hat{\tilde{L}}\left(d_j, \theta_k(t_{A_n}), t_{A_n}; \gamma, \xi\right)\right)$$
$$- \sum_{n=1}^{N_A}\left(\frac{1}{N_{\mathrm{mcs}}}\sum_{p=1}^{N_{\mathrm{mcs}}}\left(\min_{d_i}\frac{1}{N_{\mathrm{mcs}}}\sum_{q=1}^{N_{\mathrm{mcs}}}\hat{\tilde{L}}\left(d_j, \theta_q(t_{A_n})|\mathbf{x}_{e_p}(t_{A_n}), t_{A_n}; \gamma, \xi\right)\right)\right). \quad (24)$$

Remark 3: In practical situations, major repairs can result in changes to the physical system and alterations to the gate's degradation pattern. Additionally, actions taken during the current time step can impact all future maintenance activities. Incorporating these factors when calculating the VoI metrics will enable a more comprehensive analysis of the value of the SHM system. However, doing so would require re-running all FEM simulations and repeating diagnostics and prognostics numerous times, which is computationally prohibitive. Possible ways of overcoming these computational challenges include using a surrogate-model-based approach to accelerate the process of diagnostics and prognostics, using approximation methods such as Fisher's information matrix to enable analytical Bayesian model updating for damage diagnostics, and building a surrogate model for the overall VoI assessment. In this paper, however, we define the VoI metric under the assumption that the only action taken is shutting down and inspecting the system, without performing any significant maintenance activity unless there is damage requiring replacement of the structure. As a result, the degradation pattern and physical properties of the gate remain unchanged. The VoI obtained under this assumption can be viewed as the lower bound of the actual VoI. Therefore, the sensor placement optimization obtained in this manner is still valid.

Remark 4: We make three observations about the assumptions made regarding the costs estimation:

1. Only the decision consequence cost (Cost A) is adjusted for utility. The utility function, parametrized by (γ, ξ), is used to model the behavioral aspect or the risk perception of the decision-maker and therefore only impacts the cost of decision-making, denoted by the consequence function $\hat{L}(d_i, \theta_{\text{true}}; \gamma, \xi)$. That is, subjectivity in decision-making is incorporated using a utility function that quantifies the perception of the cost by an individual or organization, which in turn affects their decision-making. This, in turn, impacts the cost savings due to better data-informed decision-making, quantified as $C_{\text{savedLC}}(e; \gamma, \xi)$.
2. It is reasonably assumed that the present value of the investment cost (Costs B, C, and D) can be objectively obtained and is independent of the decision-maker's risk perception. Therefore, the total investment cost over the lifecycle, denoted by $C_{\text{investedLC}}(e)$, is independent of the decision-maker's risk profile or utility. Similar to the decision-maker's risk profile, the investment costs could be estimated more or less conservatively using a margin of safety factor.
3. Except for Cost D, which is incurred at the beginning of the lifecycle, Costs A, B, and C will be spread over the structure's lifecycle. The values of these costs are estimated at $t = 0$ and then inflated to obtain their future value at time t. Let the cost estimated at time $t = 0$ be denoted as the *Current Value* (CV), and the inflated cost at time $t>0$, representing the Future Value FV(t). For the rate of inflation denoted by $r(t)$, we have:

$$\text{FV}(t) = \text{CV}(1 + r(t))^t. \quad (25)$$

To accurately assess the economic impact over the structure's lifecycle, we can apply a discounting rate to these future values to obtain the corresponding present value of the cost. The time value of money principle states that money available today is worth more than the same amount in the future due to its potential earning capacity. In addition, discounting provides a more accurate present value of future cash flows, allowing for better comparison and evaluation of different investment options or strategies, especially when comparing not-so-similar SHM system designs subjected to a set of maintenance policies that have different cost structures. The present value PV(t) of the future costs at time t can be calculated by applying a discount rate $d(t)$ as follows:

$$\text{PV}(t) = \frac{\text{FV}(t)}{(1 + d(t))^t} = \text{CV}\frac{(1 + r(t))^t}{(1 + d(t))^t}. \quad (26)$$

In the proposed sensor optimization framework, we simplify the analysis by setting the discount rate $d(t) = 0$. While discounting future costs would yield a more accurate present value, our main objective is to highlight potential cost savings from sensor data. By focusing on nominal values and applying a constant inflation rate, we assume a simplified cost structure. However, it is straightforward to include the discount rate in the analysis by discounting the costs to present value, thereby keeping the framework generic and adaptable.

The rate of savings: time-normalized and unitless VoI measure

When evaluating sensor designs for its performance in terms of savings over the lifecycle, it is beneficial to establish metrics that normalize the VoI over time and are unitless. In this context, we define three metrics that can be used to gauge the VoI normalized over the structure's lifecycle: (1) average annual expected rate of savings; (2) compounded annual expected rate of savings; and (3) exponentially compounded annual expected
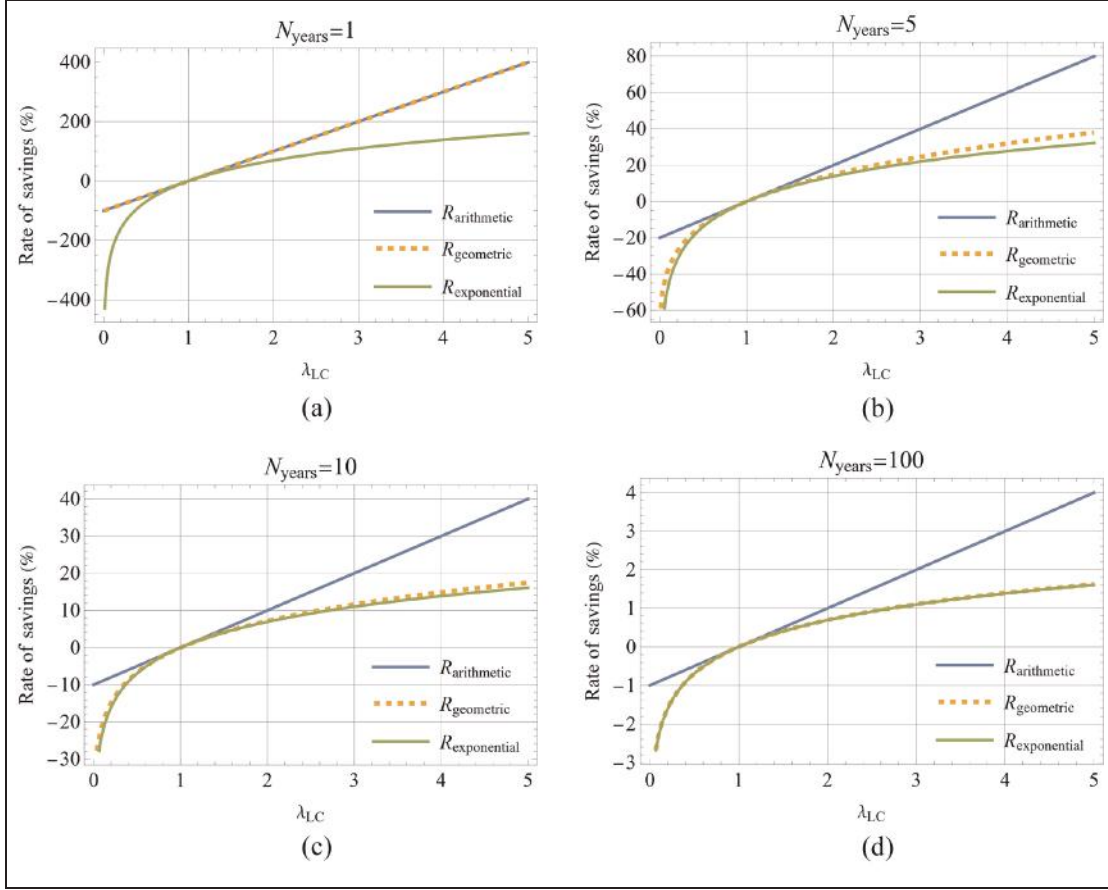
Figure 9. Various rate of savings metric simulated for different lengths of lifecycle: (a) considering lifecycle of 1 year, (b) considering lifecycle of 5 year, (c) considering lifecycle of 10 year and (d) considering lifecycle of 100 year.

rate of savings. We will investigate the overall benefit of various sensor placement designs obtained using different objective functions by evaluating these metrics in section "Life cycle cost analysis and marginal utility of additional sensors for various designs over the structure's lifecycle."

Average expected annual rate of savings, denoted by $R_{\text{arithmetic}}(e; \gamma, \xi)$, defines the net expected annual savings from the SHM design e over the structure's lifecycle of N_{years} relative to the total investment made, such that:

$$R_{\text{arithmetic}}\left(e, N_{\text{years}}; \gamma, \xi\right)$$
$$= \frac{1}{N_{\text{years}}}\left(\frac{C_{\text{savedLC}}(e; \gamma, \xi) - C_{\text{investedLC}}(e)}{C_{\text{investedLC}}(e)}\right)$$
$$= \frac{1}{N_{\text{years}}}\left(\frac{\text{EVoI}_{\text{LC}}(e; \gamma, \xi)}{C_{\text{investedLC}}(e)}\right) = \frac{1}{N_{\text{years}}}\left(\lambda_{\text{LC}}(e; \gamma, \xi) - 1\right).$$
$$(27)$$

Compounded expected annual rate of savings, denoted by $R_{\text{geometric}}\left(e, N_{\text{years}}; \gamma, \xi\right)$, is defined as:

$$R_{\text{geometric}}\left(e, N_{\text{years}}; \gamma, \xi\right) = \lambda_{\text{LC}}(e; \gamma, \xi)^{\frac{1}{N_{\text{years}}}} - 1. \quad (28)$$

Finally, the exponentially compounded expected rate of savings, denoted by $R_{\text{exponential}}(e, N_{\text{years}}; \gamma, \xi)$, is defined as:

$$R_{\text{exponential}}\left(e, N_{\text{years}}; \gamma, \xi\right) = \log\left(\lambda_{\text{LC}}(e; \gamma, \xi)^{\frac{1}{N_{\text{years}}}}\right). \quad (29)$$

We notice that all three standardized metrics are unitless (expressible in percentages) and depend solely on the ratio of the expected savings C_{savedLC} to the investment costs $C_{\text{investedLC}}$ (i.e., $\lambda_{\text{LC}}(e; \gamma, \xi)$), normalized over the number of years constituting the lifecycle. These metrics can be beneficially used when evaluating the performance of not-necessarily-similar SHM systems over an extended period.

Figure 9 illustrates the rate of savings metric as a function of λ_{LC} simulated for different lengths of the lifecycle. We observe that when $N_{\text{years}} = 1$, $R_{\text{geometric}} = R_{\text{arithmetic}}$, and as the number of years increases, $R_{\text{geometric}}$ approaches $R_{\text{exponential}}$. Since $R_{\text{geometric}}$ and $R_{\text{exponential}}$ assume the savings compound over time,

they are more constrained and stable, especially over a long period of time and for a larger expected savings to investment ratio λ_{LC}, compared to the arithmetic rate of savings $R_{arithmetic}$ which is a linear function of λ_{LC}.

Remark 5: Because information is expected to provide benefits when cost is disregarded, or at the very least, not cause harm, that is, $C_{savedLC}(e; \gamma, \xi) \geqslant 0$, we observe the lower limit on these metrics:

$$\lim_{C_{savedLC}(e;\gamma,\xi)\to 0} R_{geometric}(e; \gamma, \xi) = -1; \quad (30)$$

$$\lim_{C_{savedLC}(e;\gamma,\xi)\to 0} R_{exponential}(e; \gamma, \xi) = -\infty. \quad (31)$$

$$\lim_{C_{savedLC}(e;\gamma,\xi)\to 0} R_{arithmetic}(e; \gamma, \xi) = -\frac{1}{N_{years}}. \quad (32)$$

Similarly, the lower limit on these metrics will be reached when the cost of investment reaches a very large value, such that:

$$\lim_{C_{investedLC}(e;\gamma,\xi)\to\infty} R_{geometric}(e, N_{years}; \gamma, \xi) = -1; \quad (33)$$

$$\lim_{C_{investedLC}(e;\gamma,\xi)\to\infty} R_{exponential}(e, N_{years}; \gamma, \xi) = -\infty. \quad (34)$$

$$\lim_{C_{investedLC}(e;\gamma,\xi)\to\infty} R_{arithmetic}(e, N_{years}; \gamma, \xi) = -\frac{1}{N_{years}}. \quad (35)$$

That is, in the limiting case where the acquired information results in zero or negligible savings, it indicates a loss of 100% of the investment (as reflected in Equations (30) and (33)). In other words, the investment does not provide any benefits whatsoever. Alternatively, it can be understood as the investment losing a fraction of $1/N_{years}$ of its value every year for a duration of N_{years} years (as reflected in Equation (32) and (35)).

Remark 6: For an SHM system to be feasible over its lifecycle, we have:

$$R_{arithmetic}(e, N_{years}; \gamma, \xi) \geqslant 0; \quad (36)$$

$$R_{geometric}(e, N_{years}; \gamma, \xi) \geqslant 0; \quad (37)$$

$$R_{exponential}(e, N_{years}; \gamma, \xi) \geqslant 0. \quad (38)$$

Remark 7: We notice that the quantities $C_{savedLC}(e; \gamma, \xi)$, $C_{saved}(e, t; \gamma, \xi)$, $\tau(e; \gamma, \xi)$, $EVoI_{LC}(e; \gamma, \xi)$, $\lambda_{LC}(e; \gamma, \xi)$, $R_{arithmetic}(e, N_{years}; \gamma, \xi)$, $R_{geometric}(e, N_{years}; \gamma, \xi)$, and $R_{exponential}(e, N_{years}; \gamma, \xi)$ depend on the risk profile, parameterized by (γ, ξ) used in the decision-making process. As mentioned in Table 1, we focus our attention on three risk profiles denoted by RP1, RP2, and RP3 (in ascending order of risk-seeking behavior). Therefore, for simplicity, we may denote the

aforementioned variables using these risk profile IDs. For example, $EVoI_{LC}(e; RP1)$ quantifies the expected VoI over the lifecycle of the structure considering the risk-aversion profile RP1 with its (γ, ξ) value mentioned in Table 1.

Optimization and results

Optimal sensor design algorithm

Let $e^*_{EVoI_{LC}}$ and $e^*_{\lambda_{LC}}$ denote the optimal sensor placement design that maximizes the $EVoI_{LC}$ and λ_{LC} metric. Mathematically:

$$e^*_{EVoI_{LC}} = \underset{e\in\Omega_E}{\arg\max} \, EVoI_{LC} \quad (39)$$

$$e^*_{\lambda_{LC}} = \underset{e\in\Omega_E}{\arg\max} \, \lambda_{LC}. \quad (40)$$

Given the colossal size of the design space Ω_E, as reflected in Equation (3), we use an iterative Bayesian optimization approach to find the global optimum in a minimal number of steps, thereby reducing the sampling points and accelerating the optimization process. However, the iterative design approach presented in this paper (adding one sensor at a time until the objective function converges) may lead to sub-optimal designs, despite its computational efficiency.

For each addition of a sensor, the algorithm performs a global search for all possible sensor candidates. However, because the final design consists of sensors added iteratively and conditioned upon previously selected sensors, a greedy algorithm is used between iterations. This procedure may result in sub-optimal solutions as the sensors are added iteratively rather than being globally optimized all at once.[41] We developed this optimization algorithm in our previous work.[14,24,42] To avoid diverting readers from the main focus of the paper, which investigates the impact of different VoI metrics and risk profiles on optimal sensor design, we present the optimization algorithm used to obtain the sensor placements in Appendix "Bayesian optimization algorithm."

Results and discussion

Various sensor designs. There are multiple options for obtaining the initial design e_0, which is composed of $N_0 \geqslant 0$ sensors. One option is to randomly generate it using the Latin hypercube sampling (LHS) technique (first introduced by McKay, Beckman, and Conover in their paper[43]). Alternatively, it can be predefined based on judgment or experience. If no predefined design is available or if one prefers not to assume a random initial design, it can be set to 0. In this paper, we numerically implement the optimization algorithm without

assuming any initial design, that is, we assume that $N_0 = 0$.

For the maintenance and operations costs per month, we assume a fixed value of $C_M = C_O = 3 \times 10^{-6}$ units. Additionally, we assume the initial SHM system design cost of $C = 2 \times 10^{-5}$ units. It is important to note, for comparison purposes, that the cost of failure—incorporating loss of life, property damage, and structure replacement—is assumed to be 1 unit, which can be assigned as necessary (e.g., 1 unit can be assigned to be one million, 10 million, etc.). We further consider an annual inflation rate of 2% and simulate a lifecycle of 9 years.

We selected these values for the maintenance, operations, and SHM design costs based on the cost-classifier plots obtained in our previous paper.[5] By carefully considering the these costs, we aimed to ensure that the obtained SHM designs are subject to a sufficient financial constraint, allowing us to observe the true impact of different sensor designs on the VoI. If we had chosen a much lower cost values, the resulting SHM designs would not have been adequately constrained by the expenses, thereby limiting our ability to assess the influence of sensor designs on VoI accurately.

Conversely, opting for significantly larger values would have made it exceedingly challenging to achieve economically feasible SHM system designs. Such excessively expensive systems would not be practically feasible in real-world scenarios. Consequently, we determined that the chosen values of maintenance and operations costs strike the right balance, enabling us to conduct a comprehensive study on SHM system design. These specific values of costs are therefore deemed suitable for the objectives of this study.

For the purpose of investigation, we consider four designs for comparison:

1. Optimal design $e_{\text{EVoI}_{\text{LC}}}^*$ obtained using Equation (39)
2. Optimal design $e_{\lambda_{\text{LC}}}^*$ obtained using Equation (40)
3. Optimal design e_{KL}^* obtained by using the KL divergence objective functional (without risk-weights) proposed in section 3 of Yang et al.[25]
4. Random design e_{Random} obtained using a network of strain gauges distributed randomly across the miter gate structure, utilizing the LHS algorithm.[43]

We can categorize these designs into three classes. The first class comprises econometric-based or VoI-based optimal designs, such as $e_{\text{EVoI}_{\text{LC}}}^*$ and $e_{\lambda_{\text{LC}}}^*$. These designs are meant to maximize the monetary benefit of information gain. The second class includes information-based designs, such as e_{KL}^* and various f-divergence-based optimal designs discussed in Yang

et al.[14] These designs focus on maximizing information gain. Finally, the third class consists of random designs, denoted as e_{Random}, which are based on random selection without specific optimization criteria. We explore the influence of the number of sensors considered in the aforementioned designs on various VoI metrics by investigating different scenarios where the number of sensors, denoted by N_{sg}, takes values from the set $\{1, 2, 3, 4, 5, 6, 7, 8\}$.

Figure 10 illustrates the random design and KL-divergence-based design, considering up to 10 sensors. Figures 11, 12, and 13 show the optimal sensor design $e_{\text{EVoI}_{\text{LC}}}^*$ for risk profiles RP1, RP2, and RP3, respectively. Figures 14, 15, and 16 display the optimal sensor design $e_{\lambda_{\text{LC}}}^*$ for risk profiles RP1, RP2, and RP3, respectively.

We immediately observe several critical points directly related to the performance of various designs in terms of the VoI they provide:

1. The KL-divergence-based design is optimized to maximize information gain or minimize uncertainty. As a result, almost all sensors are placed close to the damage (loss of gap at the bottom of the gate). It is important to note that the KL-divergence-based design is not directly related to the monetary benefit of information gain, as quantified by the VoI metrics discussed in this paper.
2. The optimal designs obtained using VoI-based metrics, such as the designs $e_{\text{EVoI}_{\text{LC}}}^*$ and $e_{\lambda_{\text{LC}}}^*$, have their first sensor placed close to the damage irrespective of the risk profiles. However, the subsequent additional sensors are not *necessarily* located near the damage.
3. Another important observation is that in the case where no sensors are present (prior decision case), by definition as presented in Equation (15), EVoI_{LC} is equal to zero. This is because when there is no additional information and, by extension, no data-informed decision-making, the expected cost savings over the lifecycle identically go to zero, and the investment cost over the lifecycle is zero since no investment is made to acquire information. As seen in EVoI_{LC} versus number of added sensor plot illustrated in Figures 11, 12, and 13, when the first optimal sensor is added, there is a significant jump in the gain of EVoI_{LC} value, that is, $\text{EVoI}_{\text{LC}} > 0$ for the first added sensor. However, the marginal benefit of adding subsequent sensors in terms of their economic benefit diminishes due to the law of diminishing returns.[44,45]
4. This diminishing effect is even more pronounced in the λ_{LC}-based designs, where the λ_{LC} metric and the corresponding rate of savings $R_{\text{geometric}}$ are highest for the first sensor. Each additional sensor,
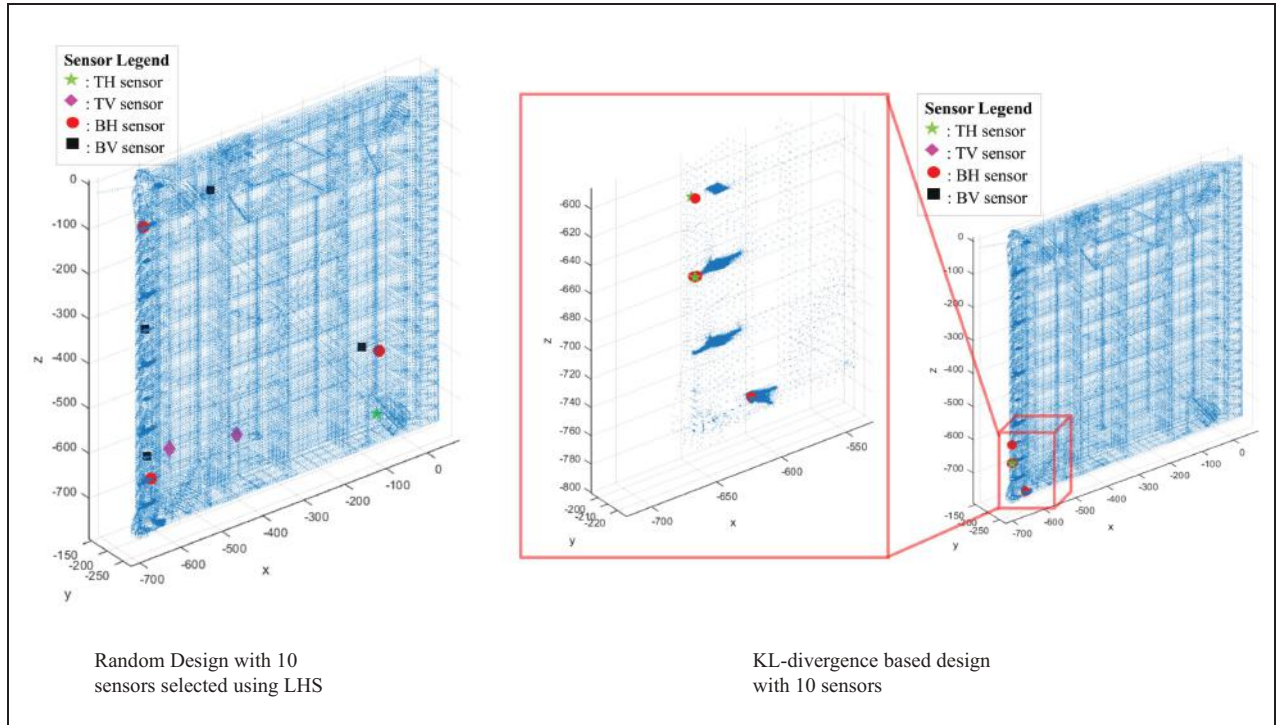
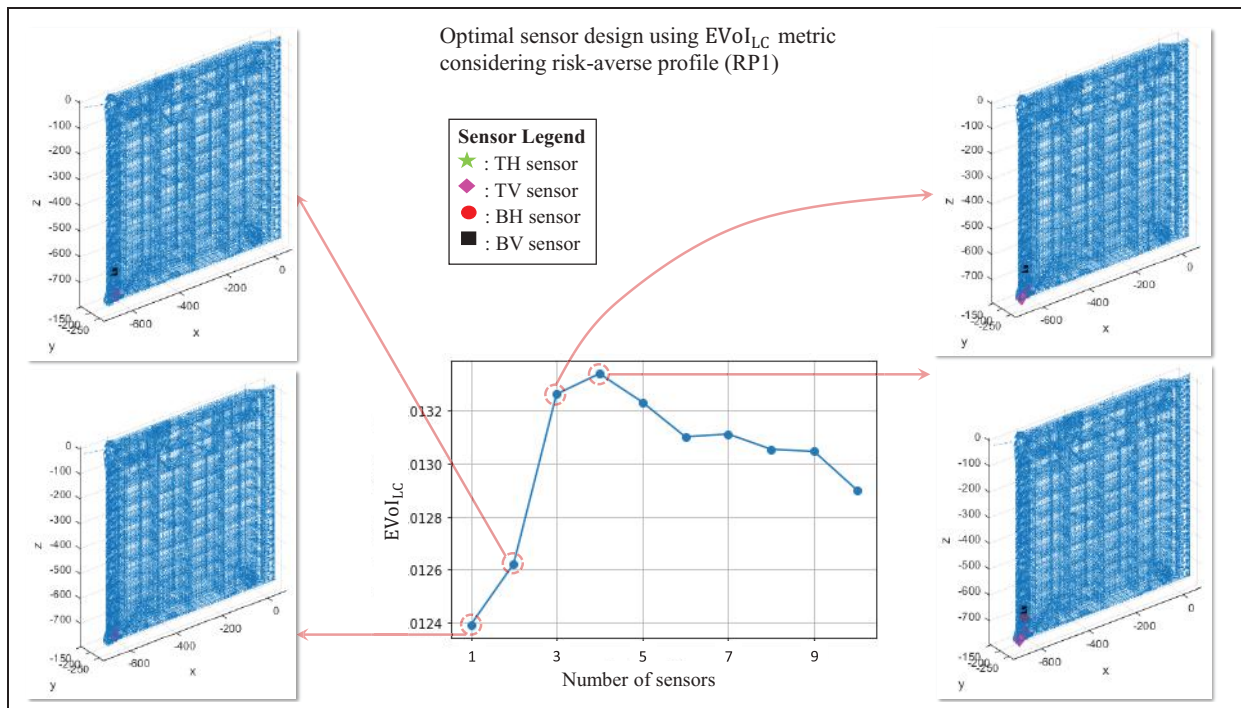**Figure 10.** Random design (left) and KL-divergence-based design (right).

Figure 11. Optimal design $e^*_{EVoI_{LC}}$ considering risk-averse profile RP1.

which incurs extra costs, decreases the expected economic benefit gained from acquiring additional information causing the λ_{LC} curve to decay as number of sensors increases. Therefore, in VoI-
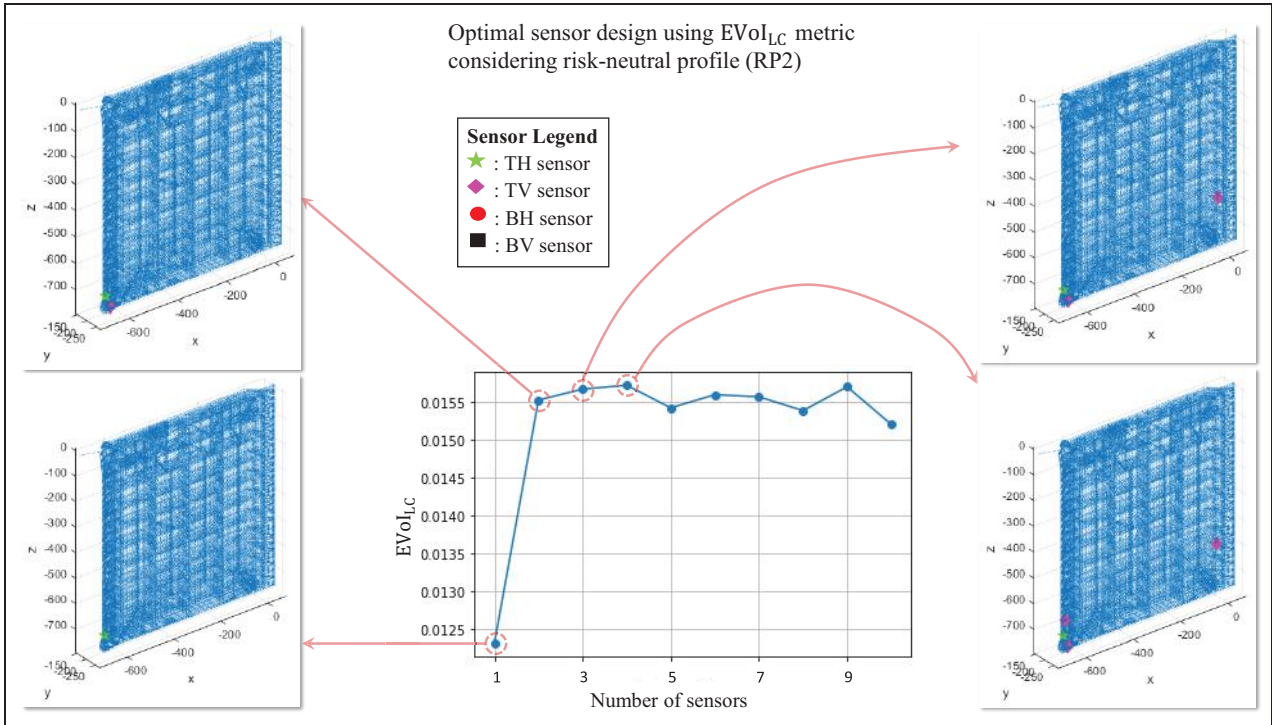
Figure 12. Optimal design $e^*_{EVoI_{LC}}$ considering risk-neutral profile RP2.
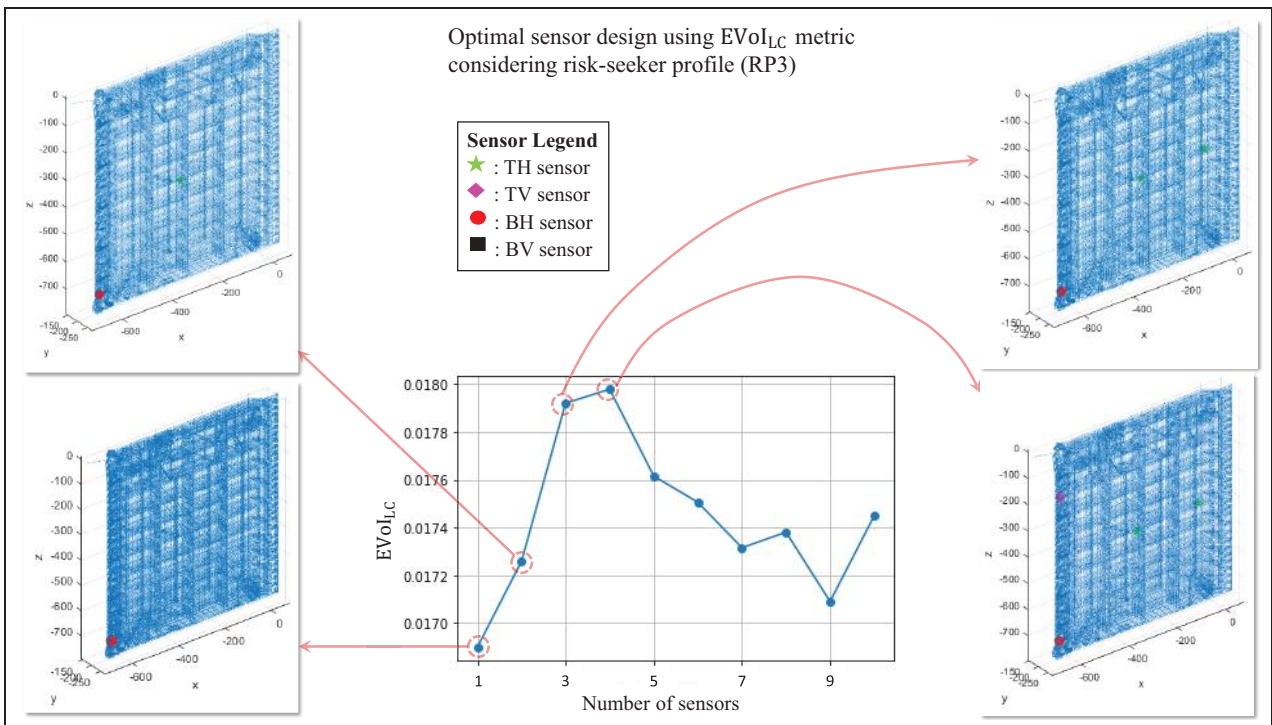
Figure 13. Optimal design $e^*_{EVoI_{LC}}$ considering risk-seeker profile RP3
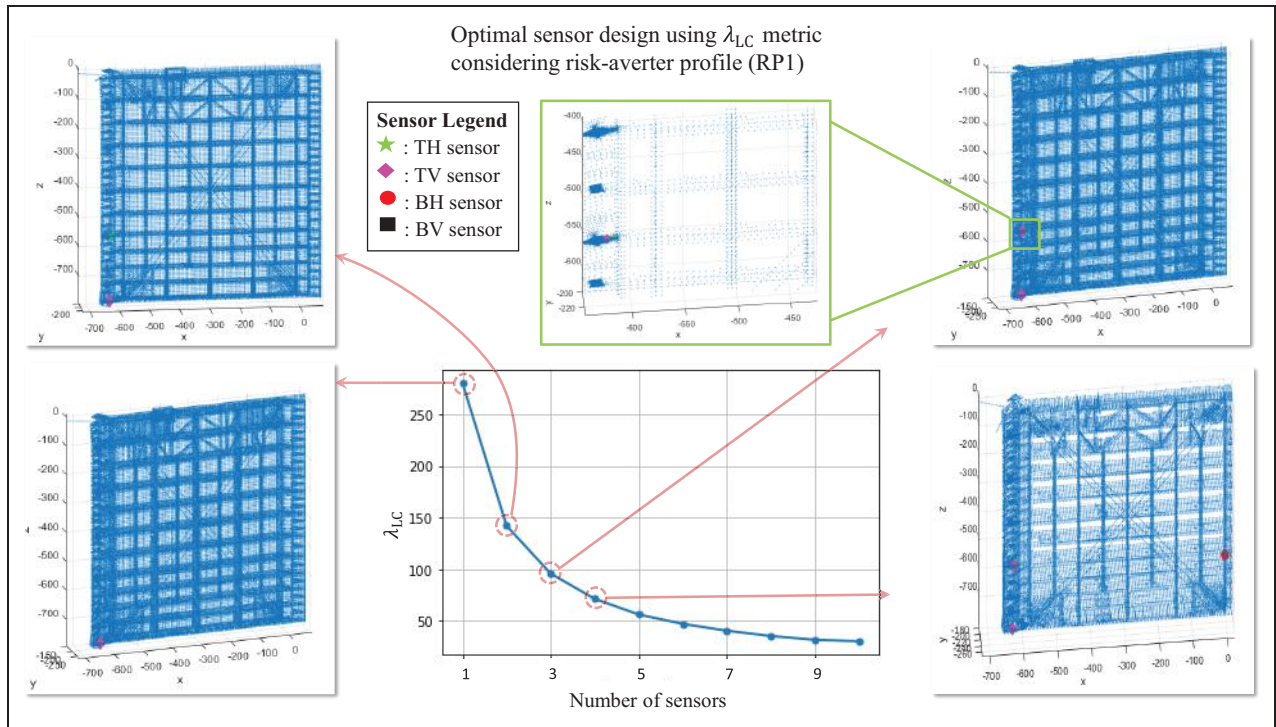
Figure 14. Optimal design $e^*_{\lambda_{LC}}$ considering risk-averse profile RP1.
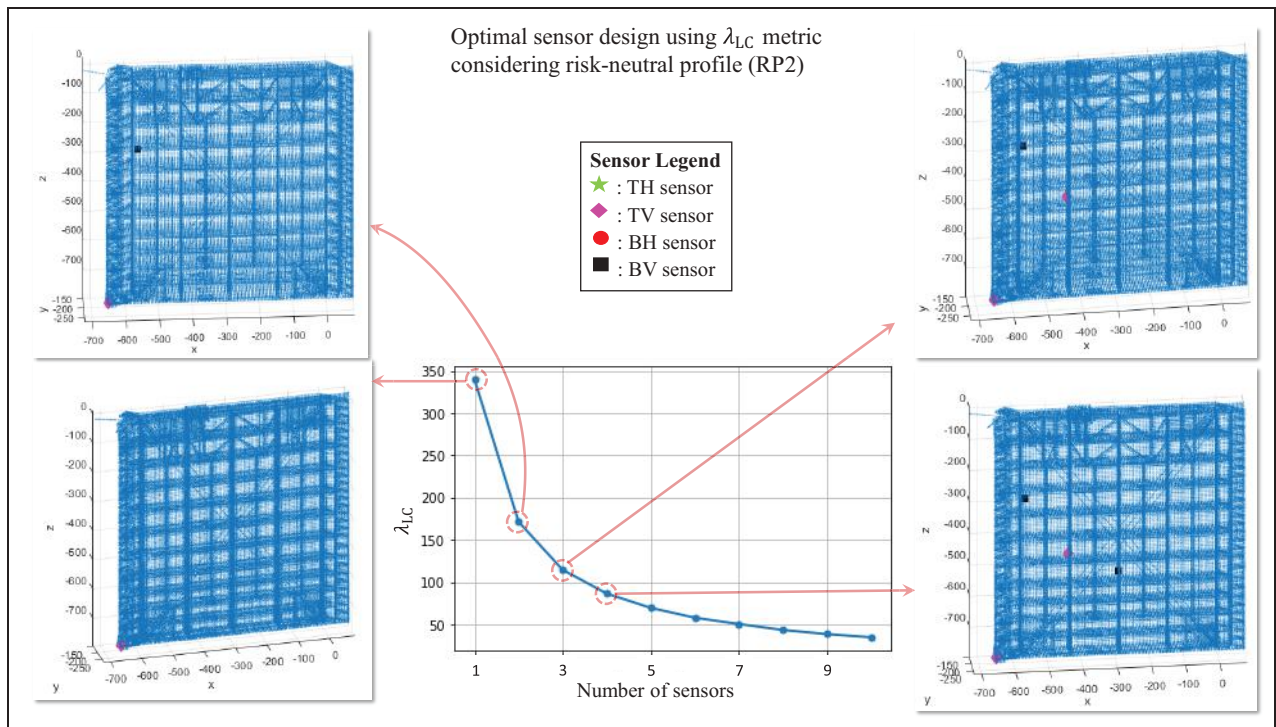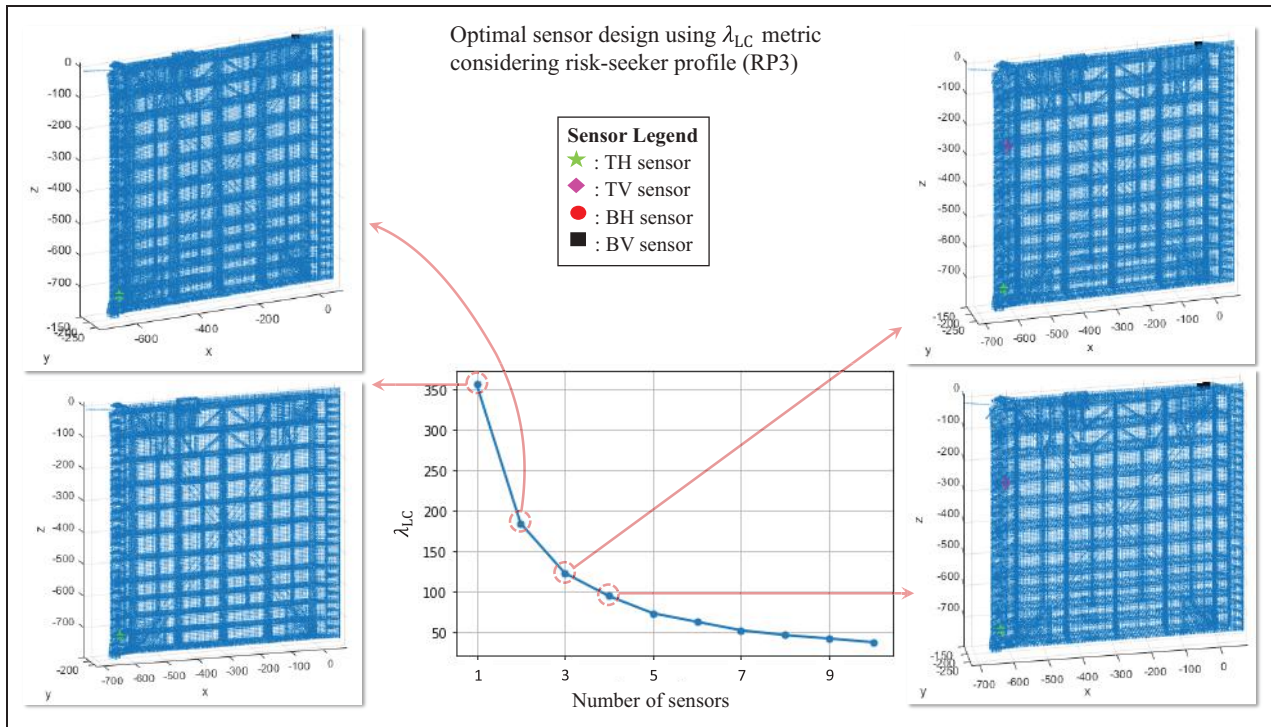

Figure 15. Optimal design $e^*_{\lambda_{LC}}$ considering risk-neutral profile RP2.

based designs, the first optimal sensor holds the most significant importance and provides

maximum marginal utility. In some cases, the incremental benefit offered by the additional

Figure 16. Optimal design $e^*_{\lambda_{LC}}$ considering risk-seeker profile RP3.

sensors beyond the first one may not compensate for the additional cost they incur.

5. However, unlike the VoI based designs, when it comes to KL-divergence-based design, although the marginal gain in information from the additional sensors after the first one diminishes, it is still optimized to maximize the information gain. As a consequence, even the additional sensors after the first one are positioned closer to the damage and will not lead to detrimental decision-making even when the most valuable first sensor is excluded.

The effect of information on the cost of decision-making. It is of importance to investigate the performance of different sensor designs in terms of cost savings resulting from data-informed decision-making over time, without considering the cost of the SHM system itself. Recall from Remark 1 that $C_{saved}(e, t; \gamma, \xi)$ represents the expected cost saved by virtue of making a data-informed decision using the information gathered using the sensor placement design e at time t and that $C_{saved}(e, t; \gamma, \xi) \geqslant 0$. It is useful to study the trends and characteristics of $C_{saved}(e, t; \gamma, \xi)$ for various optimal sensor placement designs (reported in units of *Normalized Cost* defined in section "The base cost model") as a function of time t and for different risk profiles (parameterized by (γ, ξ)). Figures 17, 18, and

19 illustrate the cost saved as a consequence of choosing optimal maintenance strategy at the various instance of time based on newly acquired strain data for the three risk profiles, considering the information obtained from the first sensor, from the first four sensors, and from the first eight sensors respectively. We make the following observations:

1. In all cases, we observe that C_{saved} is greater than or equal to zero, except for numerical errors (as mentioned in Remark 1). This is the consequence of the fact that unbiased information, even with its inherent uncertainty, is always valuable when it is freely accessible.

2. Additionally, the cost savings increase up to a certain damage level, after which they decrease. The value of C_{saved} evaluates the economic benefit of arriving at a data-informed maintenance decision as a consequence of having an SHM system installed compared to the decisions we would have made using the prior decision analysis. However, beyond a certain gap-length value, the maintenance decision obtained using the posterior decision analysis is the same as the decision obtained using the prior decision analysis. For instance, when the gate is approaching the end of its lifecycle and nearing the critical failure level, it is obvious that an engineer with any risk profile
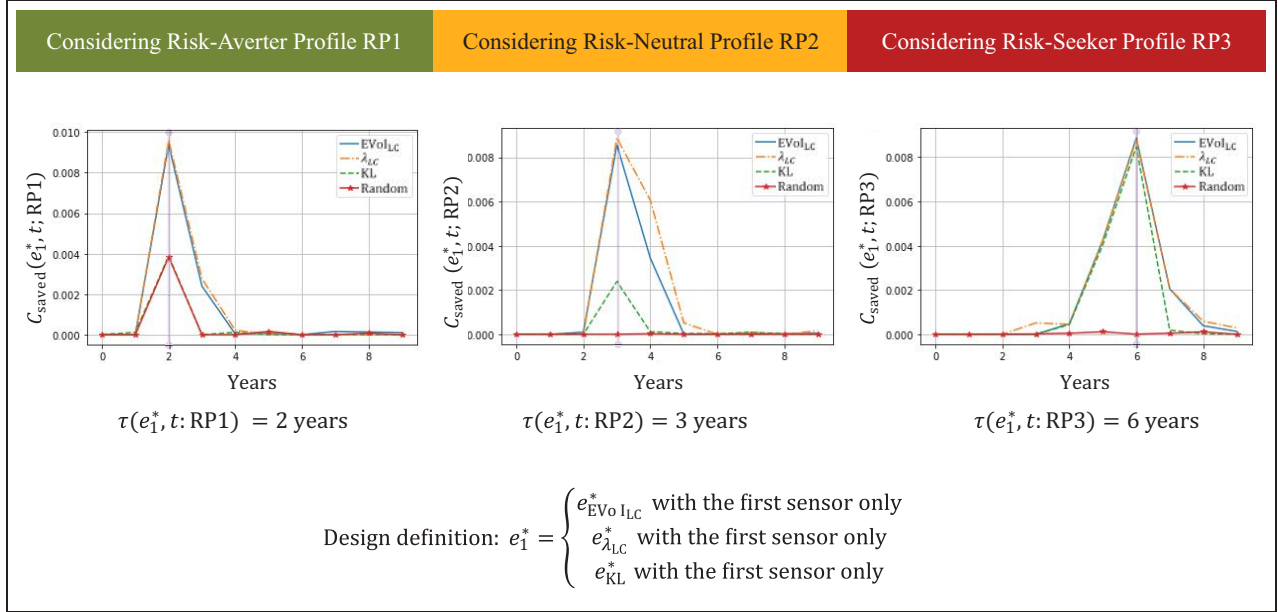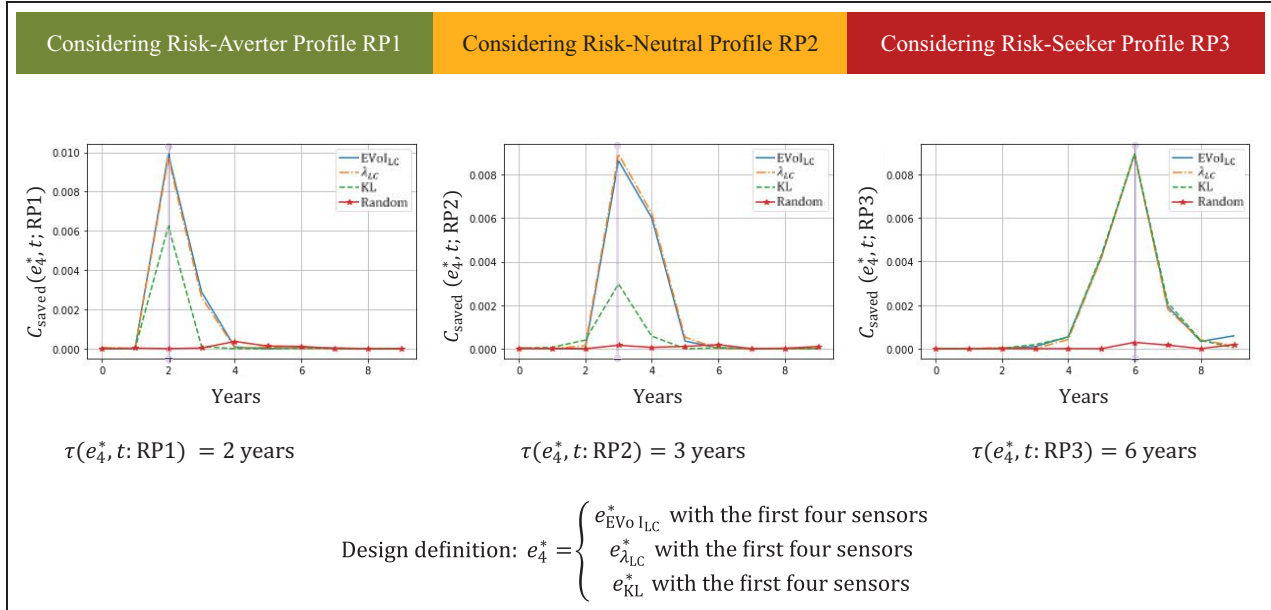
Figure 17. Comparison of the expected cost savings, $C_{\text{saved}}(e_1^*, t; \gamma, \xi)$ from various optimal designs consisting of the first optimal sensor only (generically denoted by e_1^*), with a random design consisting of only one sensor.

would choose to perform maintenance. In such obvious decisions, SHM is not necessarily useful at that instance in time.

3. We observe a shift in the peaks of C_{saved} toward higher gap lengths as the intensity of risk-seeking increases. Figures 17, 18, and 19 also mention the time when peak savings occur, denoted by $\tau(e; \gamma, \xi)$ and defined in Equation (23). This shift occurs because the increase in risk-aversion of the decision-maker (or decrease in risk-seeking behavior) decreases the threshold of the gap beyond which it becomes obvious to the decision-maker that the structure is damaged, and the SHM system does not offer much benefit.

4. For VoI-based designs, it is more likely that there are more sensors close to the damage for the risk-averse profile than for the risk-neutral and risk-seeking profiles (as seen in Figures 11, 12, 13, 14, 15, and 16). One plausible reason for this observation is that the risk-neutral profile leads to information-led cost savings in the early phase of the structure's lifespan. However, the damage is not very prominent in the early phase, and more information is required to sufficiently capture the damage in order to make accurate inferences and, eventually, informed maintenance decisions. On the other extreme, the risk-seeking profile becomes active toward the end of the structure's life when the damage is much more prominent. Therefore,

only one well-placed sensor is enough to make a useful decision.

5. The performance of the optimal designs $e_{\text{EVoI}_{\text{LC}}}^*$, $e_{\lambda_{\text{LC}}}^*$, and e_{KL}^* is better than that of the random design e_{Random} in terms of information-led cost savings. The performance of the designs $e_{\text{EVoI}_{\text{LC}}}^*$ and $e_{\lambda_{\text{LC}}}^*$ is very similar. The C_{saved} curve for the KL-divergence-based design approaches the VoI-based designs as the number of sensors increases, but it never exceeds the VoI-based designs.

6. The performance of the KL-divergence-based design improves as we consider a greater number of sensors. On the other hand, the performance of the VoI-based design does not change significantly as the number of sensors increases. This is because the first sensor contains most of the necessary information required to make an optimal decision. This means that the first sensor provides maximum marginal utility, and the marginal benefit of the sensors excluding the first one is not meaningful when it comes to increasing the monetary VoI since additional sensors come with the penalty of additional SHM cost.

Life cycle cost analysis and marginal utility of additional sensors for various designs over the structure's lifecycle. In Tables A1 to A18 of Appendix A, we provide the values of several VoI metrics, namely EVoI_{LC}, λ_{LC}, $R_{\text{arithmetic}}$,
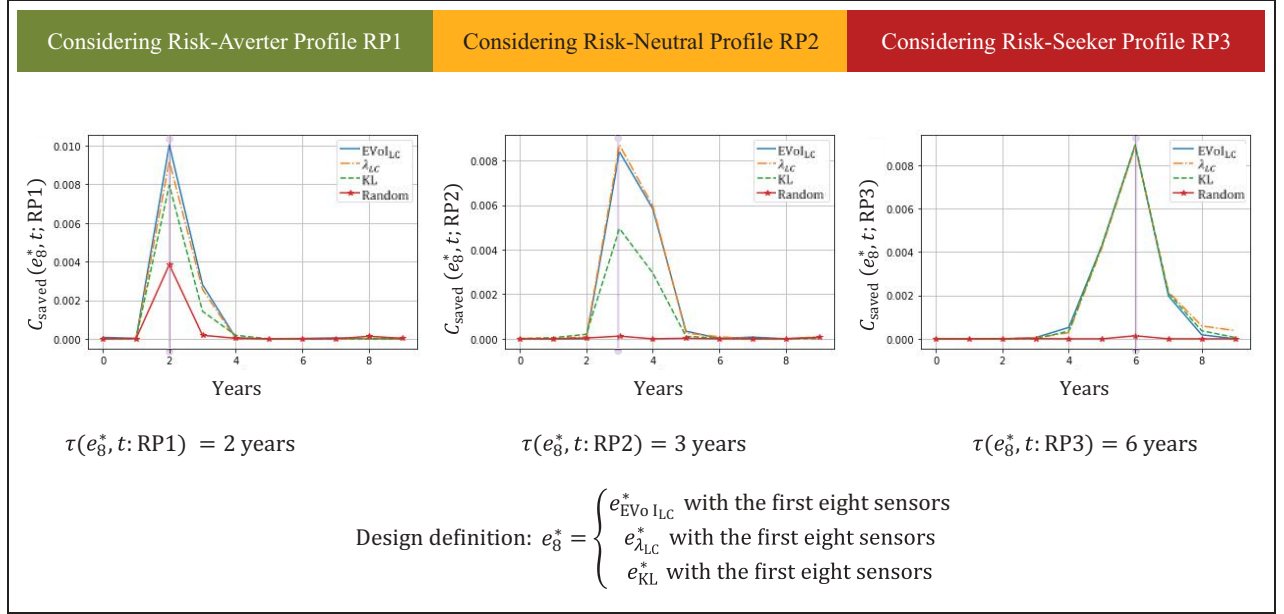
Figure 18. Comparison of the expected cost savings, $C_{\text{saved}}(e_4^*, t; \gamma, \xi)$ from various optimal designs consisting of the first four optimal sensor only (generically denoted by e_4^*), with a random design consisting of only one sensor.

$R_{\text{geometric}}$, and $R_{\text{exponential}}$ for different sensor network designs. These metrics are calculated for three specific risk profiles. In this section, we primarily focus on the annual compounded rate of savings, denoted as $R_{\text{geometric}}$, which serves as a key metric for evaluating different designs of SHM systems as long-term investments throughout a structure's lifecycle.

The metrics $R_{\text{geometric}}$ and $R_{\text{exponential}}$ offer a standardized measure that quantifies the compounded growth rate (although with slightly different definitions) over an extended period, enabling us to assess the accumulated savings over many years. Although $R_{\text{geometric}}$ and $R_{\text{exponential}}$ assume compounding of savings over time, it is important to note that in this case, the savings today do not influence the savings tomorrow. However, this characteristic renders $R_{\text{geometric}}$ and $R_{\text{exponential}}$ to be more constrained and stable compared to the arithmetic rate of savings $R_{\text{arithmetic}}$, especially when the SHM system is very profitable, that is, when $\lambda_{\text{LC}} \gg 1$. Tables A1 to A18 of Appendix A demonstrates demonstrates that changes in the value of $R_{\text{arithmetic}}$ exhibit greater sensitivity to variations in C_{savedLC} compared to $R_{\text{geometric}}$ and $R_{\text{exponential}}$. However, when the SHM system is not feasible, a well-defined lower bound of $R_{\text{geometric}}$ (see Equation (30) and (33)) makes it a more preferable metric than $R_{\text{exponential}}$ (see Equation (31) and (34)). All these characteristics make $R_{\text{geometric}}$ the best metric to evaluate the lifecycle benefit of an SHM system.

Figure 20, which consists of a 2D representation in Figure 20a and a 3D representation in Figure 20b, illustrates the compounded annual rate of expected saving $R_{\text{geometric}}$ for various designs, risk profiles, and numbers of sensors, starting from the first sensor (which is the most important sensor in an optimal design). We make the following observations:

1. As seen in Figure 20a, all the values of $R_{\text{geometric}}$ for $e_{\text{EVoI}_{\text{LC}}}^*$, $e_{\lambda_{\text{LC}}}^*$, and e_{KL}^* are in the feasible region. The VoI-based optimal designs, $e_{\text{EVoI}_{\text{LC}}}^*$ and $e_{\lambda_{\text{LC}}}^*$, perform the best for any number of sensors and any risk profile considered. The $R_{\text{geometric}}$ surface in Figure 20b for these designs is above the surface for the e_{KL}^* design, indicating their outperformance. Information-based design also leads to a feasible SHM system. The performance of the random design, e_{Random}, is *random* since the sensors are randomly selected and not optimized for any target objective. Additionally, they are not conditioned upon the information acquired from the previous sensors.

2. As we include a greater number of sensors into an optimal design, $R_{\text{geometric}}$ decreases for all risk profiles. This is indicative of the first sensor carrying maximum marginal utility in terms of cost benefit. The benefit from the additional information acquired by sensors added after the first sensor does not compensate for their additional cost. This

Figure 19. Comparison of the expected cost savings, $C_{\text{saved}}(e_8^*, t; \gamma, \xi)$ from various optimal designs consisting of the first eight optimal sensor only (generically denoted by e_8^*), with a random design consisting of only one sensor.

fact is clearly reflected in various $R_{\text{geometric}}$ curves in Figure 20a, as well as by the downward sloping $R_{\text{geometric}}$ surface in the direction of increasing number of sensors for $e_{\text{EVoI}_{\text{LC}}}^*$, $e_{\lambda_{\text{LC}}}^*$, and e_{KL}^* designs in Figure 20b.

3. We also observe that for VoI-based designs, $e_{\text{EVoI}_{\text{LC}}}^*$ and $e_{\lambda_{\text{LC}}}^*$, $R_{\text{geometric}}$ increases as the risk-seeker behavior increases. Recall that the risk-seeker profile tends to take action only where there is a real need for it, which is toward the end of the life of the structure. By doing so, it tends to save costs. Since VoI-based metrics are explicitly dependent on the risk profiles, this pattern is expected. This fact is clearly reflected in Figure 20a and 20b, which show upward sloping $R_{\text{geometric}}$ curves and surfaces in the direction of increasing risk-seeker profile for the designs $e_{\text{EVoI}_{\text{LC}}}^*$, and $e_{\lambda_{\text{LC}}}^*$.

It is of interest to investigate the marginal utility of the sensors excluding the first sensor. For that, we consider Figures 21 and 22 that illustrate the compounded annual rate of expected saving $R_{\text{geometric}}$ for various designs, risk profiles, and numbers of sensors excluding the first sensor. We make the following observations:

1. The additional sensors beyond the first sensor do not add value to VoI-based designs and instead have a detrimental effect on the overall performance. The effect is worse on $e_{\lambda_{\text{LC}}}^*$ than on $e_{\text{EVoI}_{\text{LC}}}^*$. The $e_{\text{EVoI}_{\text{LC}}}^*$ design leads to positive values of

$R_{\text{geometric}}$ for certain combinations of the number of sensors and risk profiles. However, $e_{\lambda_{\text{LC}}}^*$ without the first sensor starts behaving like a random design and mostly leads to nonfeasible SHM system.

2. Excluding the first sensor decreases the performance of information-based design $e_{\lambda_{\text{KL}}}^*$ as well but it still leads to a feasible SHM design for all risk profiles as well as number of sensors considered. This can be seen in Figures 21b and 22b where the $R_{\text{geometric}}$ surface for e_{KL}^* design consistently stays positive. This is because, in contrast to VoI-based designs, KL-divergence-based designs prioritize maximizing information gain and positioning additional sensors closer to the damage, even if the marginal gain in information decreases. This ensures that excluding the most valuable first sensor does not result in detrimental inference of damage and subsequently decision-making, as all subsequent sensors are still optimized for maximizing information gain.

Summary and conclusion

This paper presents a framework for sensor optimization based on the concept of VoI. The framework aims to maximize the overall benefit of information obtained through an SHM system throughout its lifecycle. The objective is to design an SHM system that generates significant cost savings through data-informed
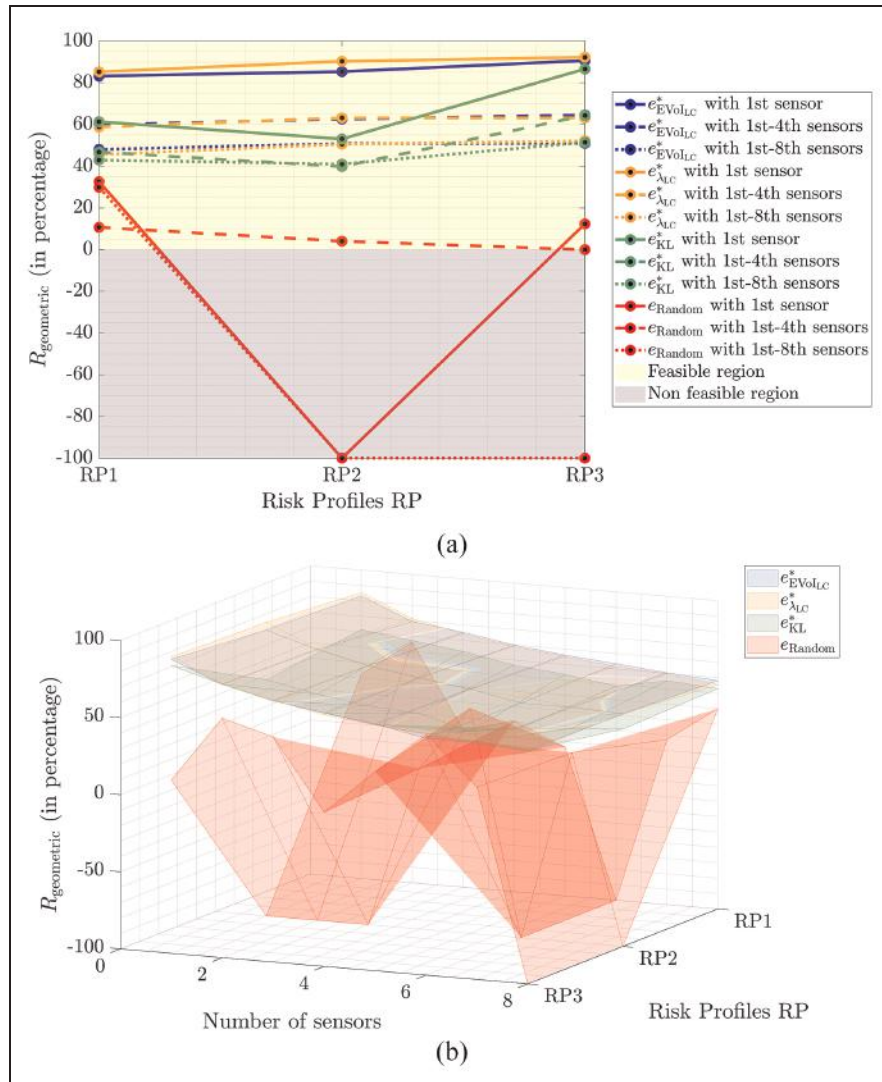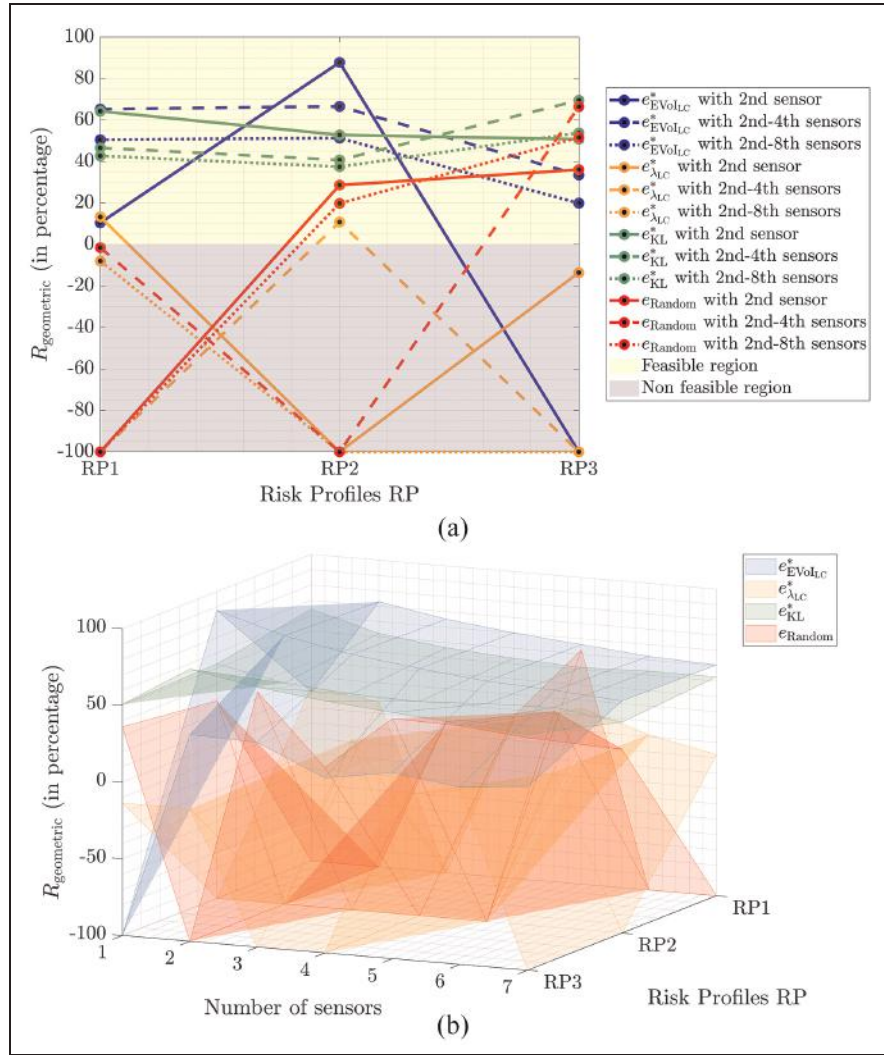
Figure 20. Compounded rate of savings $R_{\text{geometric}}$ for various designs, risk profiles, and number of sensors starting from the first sensor: (a) 2D plot: $R_{\text{geometric}}$ for various designs, risk profiles, and number of sensors and (b) 3D illustration: $R_{\text{geometric}}$ for various designs, risk profiles, and number of sensors.

decision-making while considering the expenses associated with designing, installing, operating, maintaining, and other related costs over the structure's lifecycle. Since each structure is unique with very specific design needs, suitability and accessibility of sensors, cost structures, environmental and loading conditions, modeling capabilities, and damage types, the design strategy detailed in this paper and the conclusions drawn focus on miter gate structures or structures with similar characteristics. With that in mind, we believe that this paper makes a substantial contribution to the design strategy for SHM systems, and the presented design approach, although focused on the miter gate structure, can in principle be extended to other structures.

We explore two VoI-based designs: one that maximizes the expected VoI over the structure's lifecycle, and the other that maximizes the ratio of expected savings over the lifecycle to the investment in running an SHM system. We compare these VoI-based designs with the information-based design that maximizes the gain in information quantified by KL divergence, as well as with the random design obtained by randomly selecting sensors using LHS. Additionally, we propose three time-normalized, unitless metrics, generically called the rate of expected savings, which are especially useful when quantifying the value of an SHM system over many years. We use the compounded annual rate of expected savings to compare the performance of four sensor placement designs (two VoI-based, one

Figure 21. Compounded rate of savings $R_{\text{geometric}}$ for various designs, risk profiles, and number of sensors starting from the second sensor (ignoring the first sensor): (a) 2D plot: $R_{\text{geometric}}$ for various designs, risk profiles, and number of sensors (ignoring the first sensor) and (b) 3D illustration: $R_{\text{geometric}}$ for various designs, risk profiles, and number of sensors (ignoring the first sensor).

information-based, and one random) for the complex miter gate structure simulated under an assumed maintenance policy and investigate the impact of different risk profiles on the performance of these designs.

We draw three conclusions from our study. First, all optimal designs, whether VoI-based or information-based, consistently outperform random designs. Random design relies on chance, and while it is possible for one of the randomly chosen sensors to provide good inference of structural damage, it cannot be attributed to intentional design efforts. In contrast, the optimal designs, based on either VoI or information criteria, are intentionally crafted to maximize performance and reliably enable a feasible SHM system. By leveraging systematic design principles, these optimal approaches on the chosen case study of the miter gate

structure ensure superior results compared to relying solely on chance occurrences.

Second, the performance of VoI-based design in terms of maximizing cost savings increases as the decision-maker's risk-seeking behavior intensifies. This is because the VoI-based objective functions are directly influenced by risk profiles, and risk-seeking individuals tend to take action only when there is a genuine need for it, typically toward the end of the structure's lifespan. By doing so, they effectively reduce decision costs.

Finally, the most important conclusion of the study is that, for all optimal designs, whether VoI-based or information-based, the first sensor provides the maximum marginal utility in terms of maximizing cost savings over the structure's lifecycle relative to the total investment. Additionally, as a result of the law of
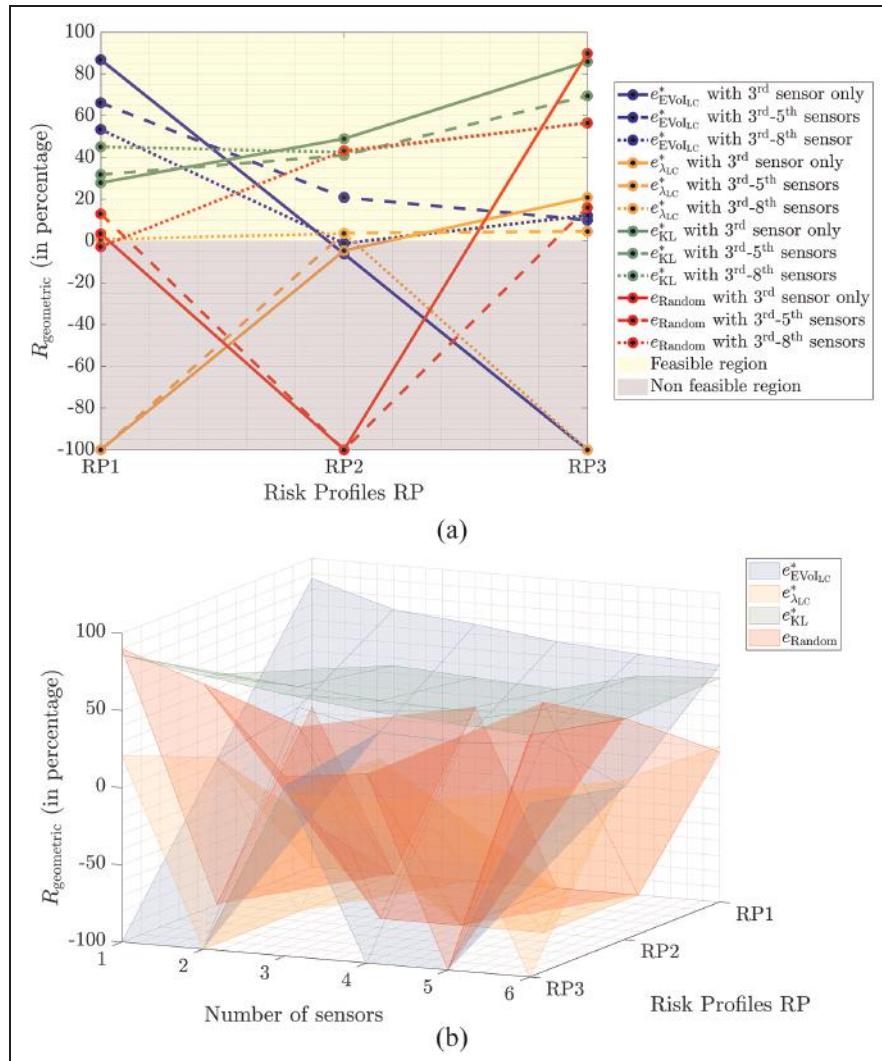
Figure 22. Compounded rate of savings $R_{\text{geometric}}$ for various designs, risk profiles, and number of sensors starting from the third sensor (ignoring the first and the second sensor): (a) 2D plot: $R_{\text{geometric}}$ for various designs, risk profiles, and number of sensors (ignoring the first and the second sensor) and (b) 3D illustration: $R_{\text{geometric}}$ for various designs, risk profiles, and number of sensors (ignoring the first and the second sensor).

diminishing return, the marginal benefit of the sensors excluding the first one is not significant when it comes to increasing the monetary VoI since additional sensors incur additional SHM costs. This is because the first sensor contains most of the necessary information required to make an optimal decision. However, when it comes to the VoI-based designs, the additional sensors beyond the first sensor do not add value to VoI-based designs and instead have a detrimental effect on the overall performance. In contrast to VoI-based designs, when it comes to the information-based design, although the marginal gain in information from the additional sensors after the first one diminishes, it is still optimized to maximize the information gain. This

ensures that excluding the most valuable first sensor does not result in detrimental damage inference and subsequently decision-making, as all subsequent sensors are still optimized for maximizing information gain.

This leads us to recommend that VoI-based optimization should be used in conjunction with information-based optimization. For instance, the first sensor can be optimized to maximize the VoI, while the subsequent additional sensors, conditioned on the first sensor, can be obtained by maximizing information gain. In practice, it is advisable to have multiple sensors because they can malfunction, and this arrangement increases the likelihood of avoiding poor decisions if the critical first sensor fails.

The proposed formulation can be further strengthened by considering other variables in the design framework, such as: (a) incorporating model uncertainty by considering distributions of model parameters and including these uncertainties in the definition of Bayes risk. This means that while defining the expected value of the quantity of interest, whether it be VoI or information gain, we account for the uncertainty in the simulated model of the structure. This will also average out possible model bias and inevitable skewness in structural properties introduced during construction; (b) in the proposed framework, we assumed a particular risk profile for the decision-maker (such as an organization). However, an organization consists of many decision-makers (inspectors and engineers) with different risk profiles. This distribution of risk profiles can also be considered while defining the objective function for sensor optimization; (c) in the proposed framework, the VoI was calculated in the pre-posterior stage (or during the initial design stage) considering the entire lifecycle of the structure. The sensors obtained from this design would be the first set of sensors installed on the structure. However, once the sensors are installed, the acquired information can be used for both diagnostics and prognostics, which in turn can be helpful in probabilistically predicting the future state of the structure. This prediction can inform maintenance strategies that consider not only the current state of the structure but also its remaining useful life. A natural extension of this idea for sensor optimization is to develop an optimization framework that starts with pre-posterior design and then updates over time based on the information acquired by the installed sensors; (d) in the current work, the damage was assumed to be a one-dimensional scalar quantity. In most practical problems, damage is a multidimensional variable. Extending this framework to a multidimensional damage scenario would be a major contribution, but it is admittedly a very challenging task that can be investigated in the future.

Declaration of conflicting interests

The author(s) declared no potential conflicts of interest with respect to the research, authorship, and/or publication of this article.

Funding

ORCID iDs

Zhen Hu (iD) https://orcid.org/0000-0003-1661-515X
Michael D. Todd (iD) https://orcid.org/0000-0002-4492-5887

References

1. Farrar CR and Worden K. *Structural health monitoring: a machine learning perspective*. Chichester, West Sussex, UK Wiley, 2012.
2. Thöns S. On the value of monitoring information for the structural integrity and risk management. *Comput Aided Civ Infrastruct Eng* 2018; 33(1): 79–94.
3. Thöns S and Stewart MG. On decision optimality of terrorism risk mitigation measures for iconic bridges. *Reliab Eng Syst Saf* 2019; 188: 574–583.
4. Konakli K and Faber MH. Value of information analysis in structural safety. In: Beer M, Au S-K, and Hall JW (eds) *Vulnerability, uncertainty, and risk: quantification, mitigation, and management*, 2014, pp. 1605–1614. ASCE.
5. Chadha M, Hu Z and Todd MD. An alternative quantification of the value of information in structural health monitoring. *Struct Health Monit* 2022; 21(1): 138–164.
6. Thöns S, Chadha M, Hu Z, et al. On metrics for information value quantification. *Struct Health Monit* 2023, 2468–2475.
7. Thöns S, Caprani C, Faber MH, et al. On information value and decision analyses. *Struct Saf* 2024, 102481.
8. Kammer DC. Sensor placement for on-orbit modal identification and correlation of large space structures. *J Guidance Control Dyn* 1991; 14(2): 251–259.
9. Meo M and Zumpano G. On the optimal sensor placement techniques for a bridge structure. *Eng Struct* 2005; 27(10): 1488–1497.
10. Hu Z, Ao D and Mahadevan S. Calibration experimental design considering field response and model uncertainty. *Comput Methods Appl Mech Eng* 2017; 318: 92–119.
11. Kim T, Youn BD and Oh H. Development of a stochastic effective independence (sefi) method for optimal sensor placement under uncertainty. *Mech Syst Signal Process* 2018; 111: 615–627.
12. Gomes GF, de Almeida FA, Lopes Alexandrino PS, et al. A multiobjective sensor placement optimization for SHM systems considering fisher information matrix and mode shape interpolation. *Eng Comput* 2019; 35(2): 519–535.
13. Heydari A, Aghabozorgi M and Biguesh M. Optimal sensor placement for source localization based on rssd. *Wireless Netw* 2020; 26: 5151–5162.
14. Yang Y, Chadha M, Hu Z, et al. A probabilistic optimal sensor design approach for structural health monitoring using risk-weighted f-divergence. *Mech Syst Signal Process* 2021; 161: 107920.
15. Nath P, Hu Z and Mahadevan S. Sensor placement for calibration of spatially varying model parameters. *J Comput Phys* 2017; 343: 150–169.
16. Flynn EB and Todd MD. A bayesian approach to optimal sensor placement for structural health monitoring with application to active sensing. *Mech Syst Signal Process* 2010; 24(4): 891–903.

17. Downey A, Hu C and Laflamme S. Optimal sensor placement within a hybrid dense sensor network using an adaptive genetic algorithm with learning gene pool. *Struct Health Monit* 2018; 17(3): 450–460.

18. Wang P, Youn BD, Hu C, et al. A probabilistic detectability-based sensor network design method for system health monitoring and prognostics. *J Intell Mater Syst Struct* 2015; 26(9): 1079–1090.

19. Guratzsch RF and Mahadevan S. Structural health monitoring sensor placement optimization under uncertainty. *AIAA J* 2010; 48(7): 1281–1289.

20. Allemang RJ. The modal assurance criterion–twenty years of use and abuse. *Sound Vibr* 2003; 37(8): 14–23.

21. Yi T-H, Li H-N and Gu M. Optimal sensor placement for health monitoring of high-rise structure based on genetic algorithm. *Mathe Probl Eng* 2011; 2011: 395101.

22. An H, Youn BD and Kim HS. A methodology for sensor number and placement optimization for vibration-based damage detection of composite structures under model uncertainty. *Compos Struct* 2022; 279: 114863.

23. Hernandez EM. Efficient sensor placement for state estimation in structural dynamics. *Mech Syst Signal Process* 2017; 85: 789–800.

24. Yang Y, Chadha M, Hu Z, et al. An optimal sensor design framework accounting for sensor reliability over the structural life cycle. *Mech Syst Signal Process* 2023; 202: 110673.

25. Yang Y, Chadha M, Hu Z, et al. An optimal sensor placement design framework for structural health monitoring using bayes risk. *Mech Syst Signal Process* 2020; 168: 108618.

26. Chadha M, Yang Y, Hu Z., et al. Evolutionary sensor network design for structural health monitoring of structures with time-evolving damage. *Struct Health Monitoring* 2023; 2023: 691–697.

27. Malings C and Pozzi M. Value of information for spatially distributed systems: application to sensor placement. *Reliab Eng Syst Saf* 2016; 154: 219–233.

28. Malings C and Pozzi M. Conditional entropy and value of information metrics for optimal sensing in infrastructure systems. *Struct Saf* 2016; 60: 77–90.

29. Thelen A, Zhang X, Fink O, et al. A comprehensive review of digital twin—part 1: modeling and twinning enabling technologies. *Struct Multidiscip Optim* 2022; 65(12): 354.

30. Thelen A, Zhang X, Fink O, et al. A comprehensive review of digital twin—part 2: roles of uncertainty quantification and optimization, a battery digital twin, and perspectives. *Struct Multidiscip Optim* 2023; 66(1): 1.

31. Vega MA, Hu Z, Yang Y, et al. *Diagnosis, prognosis, and maintenance decision making for civil infrastructure: Bayesian data analytics and machine learning*. Cham, Switzerland: Springer, 2022.

32. Chadha M, Ramancha MK, Vega MA, et al. The modeling of risk perception in the use of structural health monitoring information for optimal maintenance decisions. *Reliab Eng Syst Saf* 2023; 229: 108845.

33. Bolognani D, Verzobio A, Tonelli D, et al. An application of prospect theory to a SHM-based decision problem. In: *Health monitoring of structural and biological systems*. Portland, OR, USA: International Society for Optics and Photonics, 2017, p. 10170.

34. Kahneman D and Tversky A. Prospect theory: an analysis of decision under risk. *Econometrica* 1979; 47(2): 263–291.

35. Tversky A and Kahneman D. Advances in prospect theory: cumulative representation of uncertainty. *J Risk Uncertainty* 1992; 5(4): 297–323.

36. Richardson GC. Navigation locks: navigation lock gates and valves. *J Waterways Harbor Div* 1964; 90(1): 79–102.

37. Schwieterman JP, Field S, Fischer L, et al. *An analysis of the economic effects of terminating operations at the chicago river controlling works and o'brien locks on the chicago area waterway system*. Chicago, IL: DePaul University, 2010.

38. Eick BA, Treece ZR, Spencer BF Jr, et al. Automated damage detection in miter gates of navigation locks. *Struct Control Health Monit* 2018; 25(1): e2053.

39. Foltz SD. *Investigation of mechanical breakdowns leading to lock closures*. Technical Report, ERDC-CERL Champaign, United States, 2017.

40. Stock JH and Watson MW. Forecasting inflation. *J Monetary Economics* 1999; 44(2): 293–335.

41. Papadimitriou C. Optimal sensor placement methodology for parametric identification of structural systems. *J Sound Vibr* 2004; 278(4–5): 923–947.

42. Yang Y, Madarshahian R and Todd MD. Bayesian damage identification using strain data from lock gates. *Dyn Civ Struct* 2020; 2: 47–54.

43. McKay MD, Beckman RJ and Conover WJ. A comparison of three methods for selecting values of input variables in the analysis of output from a computer code. *Technometrics* 2000; 42(1): 55–61.

44. Shephard RW and Färe R. The law of diminishing returns. In: *Production theory: proceedings of an international seminar held at the University at Karlsruhe*, May–July 1973, Springer, 1974, pp. 287–318.

45. Bejan A and Bejan A. Diminishing returns. In: Bejan A (ed) *Freedom and evolution: hierarchy in nature, society and science*, 2020, pp. 123–134.

Appendix

Bayesian optimization algorithm

Unlike optimization methods that rely on gradients, Bayesian optimization does not require the objective function's derivative. Instead, it only needs a black-box model (such as a surrogate function) of the objective function to perform the optimization. Bayesian optimization has two main components: first, a surrogate function to approximately evaluate the value of objective function is developed using randomly evaluated samples of the objective function; second, an acquisition function is used to identify the next most promising candidate for updating the design.

We demonstrate the optimization process considering the $\lambda_{\text{LC}}(e)$ as the objective function. The process begins by choosing an initial design $e^*_{\text{EVoI}_{\text{LC}}}$ consisting

of $N_{sg}(e_0) = N_0 \geqslant 0$ sensors. Here, $d^{(l)}$ represents the location of lth strain gauge in the design e_0. The next step is to obtain an updated design e_1 by adding an additional sensor to e_0, such that $N_{sg}(e_1) = N_0 + 1$. To obtain the optimal e_1, we randomly sample α sensor locations using *LHS*, subjected to a space filling property, to be the candidate for the additional sensor from the unused sensors constituting the measurement space Ω_X. These locations yield α number of design samples $\tilde{e}_k$, $\forall\, k \leqslant \alpha$ each with $N_{sg}(e_1)$ sensors. We obtain the exact cost $\lambda_{LC}(\tilde{e}_k)$, $\forall\, k \leqslant \alpha$ using approach discussed in the previous section. Using the set of α additional sensor locations as input data, denoted by $\tilde{d}$, and the exact cost as output data, we train our surrogate function $\hat{\lambda}_{LC}(\tilde{d}) \sim N(\mu_{\tilde{d}}, \sigma_{\tilde{d}}^2)$. This surrogate can be used to quickly estimate a posterior probability that describes possible values for the Bayes risk at a remaining candidate location $\bar{d}$ spanning the entire design space, with mean value $\mu_{\bar{d}}$ and standard deviation $\sigma_{\bar{d}}$. We use *Expected Improvement EI* as our acquisition function that helps us locate the next most valuable candidate for the next sensor location based on the current posterior over the Bayes risk, given by

$$\mathrm{EI}(\bar{d}) = (\mu_{\bar{d}} - \lambda_{LC}^*)\Phi\left(\frac{\mu_{\bar{d}} - \lambda_{LC}^*}{\sigma_{\bar{d}}}\right) + \sigma_{\bar{d}}\phi\left(\frac{\mu_{\bar{d}} - \lambda_{LC}^*}{\sigma_{\bar{d}}}\right). \quad (A1)$$

Here, $\lambda_{LC}^* = \max_{\tilde{e}_k} \lambda_{LC}(\tilde{e}_k)$ is the *current best value* of the objective function. For all the remaining possible additional sensor location candidates, we evaluate $\mathrm{EI}(\bar{d})$. The candidate with maximum EI is the next most valuable location. Once we locate the next most valuable sensor location candidate, we get $(\alpha + 1)$th design samples. We re-train the GPR with $(\alpha + 1)$ data points, and keep adding the next most valuable location from the set of strain locations constituting Ω_X until the maximum EI is less than a tolerance value ε.

Note that the aforementioned details updates an initial design $e_0 - e_1$ by adding one additional sensor. We keep updating the designs by adding one sensor at a time until one of the following two conditions is reached:

1. The VoI converges to a constant value, that is, the design $e_I = e^*$ (with $i = I$) can be considered as the most optimal design if $\lambda_{LC}(e_I) \approx \lambda_{LC}(e_{(I-1)})$. Given an updated design $e_i = (d^{(1)}, d^{(2)}, \cdots, d^{(N_{sg}(e_i))})$ with $N_{sg}(e_i)$ number of sensors, the aforementioned steps can be generalized to obtain the updated design $e_{(i+1)}$.
2. The total number of sensors in the design reaches the maximum number of sensors limited/constrained by the decision-maker or other factors such as $\lambda_{LC}(e_i) \geqslant 1$.

Given the design e_i, the updated design $e_{(i+1)}$ can be obtained following similar exercise as described above.

Let $e_{n_{as}}$ represent the optimized sensor design with $(N_0 + n_{as})$ sensors, such that $n_{as} \leqslant N_{as}$. Here, N_{as} represents the maximum additional sensors considered over the initially assumed number of sensors N_0. The number of sensors in the final design shall then be $\leqslant (N_0 + N_{as})$. The optimal design $e_{\lambda_{LC}}^*$ is then given by:

$$e_{\lambda_{LC}}^* = \underset{e_{n_{as}}}{\arg\max} \lambda_{LC}(e_{n_{as}}). \quad (A2)$$

Algorithm 1 demonstrates the Bayesian optimization procedure to evaluate the design $e_{\lambda_{LC}}^*$.

Algorithm 1: Bayesian optimization for sensor placement.

---

1 Initialize $e_0 = (d^{(1)}, d^{(2)}, \cdots, d^{(N_0)})$;
2 for $n_{as} = 1$ **to** N_{as} **do**
3   Using LHS, randomly select α locations to be candidates for the $(N_0 + n_{as})$ sensor location, with coordinates $\mathcal{X} = (\tilde{d}^{(1)}, \tilde{d}^{(2)}, \cdots, \tilde{d}^{(\alpha)})$;
4   Obtain α number of possible designs: $\tilde{e}_k = \text{concatenate}(e_{(n_{as}+1)}, \tilde{d}^{(k)})$, for all $k \leqslant \alpha$;
5   Obtain the exact cost of all the α designs: $\Xi = (\lambda_{LC}(\tilde{e}_1), \lambda_{LC}(\tilde{e}_2), \cdots, \lambda_{LC}(\tilde{e}_\alpha))$;
6   **while** $i = 1$ **or** $maxEI < \epsilon$ **do**
7   Construct the GPR model for $\hat{\lambda}_{LC}(\cdot)$ trained using $(\mathcal{X}, \Xi)$;
8   For all the remaining strain locations $(\bar{d}^{(1)}, \bar{d}^{(2)}, \cdots, \bar{d}^{(\beta)})$, where $\beta = (N_{Total-Sensors} - (N_0 + n_{as} - 1) - \alpha)$, obtain β number of possible designs: $\bar{e}_m = \text{concatenate}(e_{(n_{as}+1)}, \bar{d}^{(m)})$, for all $m \leqslant \beta$;
9   Obtain the cost $\hat{\lambda}_{LC}(\bar{d}^{(m)})$ for all $m \leqslant \beta$ designs using GPR developed before;
10   Obtain the current best $\lambda_{LC}^* = \max \Xi$;
11   Obtain the Expected Improvement for all the β designs using:

$$EI(\bar{d}^{(m)}) = (\mu_{\bar{d}^{(m)}} - \lambda_{LC}^*)\Phi\left(\frac{\mu_{\bar{d}^{(m)}} - \lambda_{LC}^*}{\sigma_{\bar{d}^{(m)}}}\right) + \sigma_{\bar{d}^{(m)}}\phi\left(\frac{\mu_{\bar{d}^{(m)}} - \lambda^*}{\sigma_{\bar{d}^{(m)}}}\right),$$

where $m \leqslant \beta$;

12   Obtain:

$$maxEI = \max_{\bar{x}^{(m)}}(EI(\bar{d}^{(m)}))$$
$$\bar{d} = \arg\max_{\bar{x}^{(m)}}(EI(\bar{d}^{(m)}))$$
$$\bar{e} = \text{concatenate}(e_{(n_{as}+1)}, \bar{d})$$

Evaluate the exact cost $\lambda_{LC}(\bar{e})$
13   Update:

$$\mathcal{X} = \text{concatenate}(\mathcal{X}, \bar{d})$$
$$\tilde{e}_{(\alpha+i)} = \bar{e}$$
$$\Xi = \text{concatenate}(\Xi, \lambda_{LC}(\bar{e}))$$

       $i = i + 1$
14   **end**
15   Update the sensor design: $e_{n_{as}} = \text{concatenate}(e_{n_{as}-1}, \bar{d})$
16 end
17 Obtain: $e_{\lambda_{LC}}^* = \arg\max_{e_k} \lambda_{LC}(e_k)$, where, $k \leqslant N_{as}$;

Cost data considering sensors starting with the first sensor

In the data reported here, $ denotes normalized cost. Specifically, C_{savedLC}, $C_{\text{investedLC}}$, and EVoI_{LC} are expressed in units of normalized cost.

Table A1. Costs and various VoI metrics for risk-averse profile and the first sensor.

Risk averse profile considering sensors designs consisting of the first sensor.

Designs	C_{savedLC} (in \$)	$C_{\text{investedLC}}$ (in \$)	EVoI_{LC} (in \$)	λ_{LC} (unitless)	$R_{\text{arithmetic}}$ (in %)	$R_{\text{geometric}}$ (in %)	$R_{\text{exponential}}$ (in %)
$e^*_{\text{EVoI}_{\text{LC}}}$	1.10E-02	4.72E-05	1.09E-02	232.96	2577.32	83.24	60.57
$e^*_{\lambda_{\text{LC}}}$	1.21E-02	4.72E-05	1.21E-02	257.17	2846.33	85.27	61.66
e^*_{KL}	3.49E-03	4.72E-05	3.45E-03	74.03	811.41	61.33	47.83
e_{Random}	5.97E-04	4.72E-05	5.49E-04	12.65	129.41	32.57	28.19

Table A2. Costs and various VoI metrics for risk-averse profile and the first four sensors.

Risk averse profile considering sensors designs consisting of the first four sensors

Designs	C_{savedLC} (in \$)	$C_{\text{investedLC}}$ (in \$)	EVoI_{LC} (in \$)	λ_{LC} (unitless)	$R_{\text{arithmetic}}$ (in %)	$R_{\text{geometric}}$ (in %)	$R_{\text{exponential}}$ (in %)
$e^*_{\text{EVoI}_{\text{LC}}}$	1.28E-02	1.89E-04	1.26E-02	68.01	744.60	59.82	20.36
$e^*_{\lambda_{\text{LC}}}$	1.21E-02	1.89E-04	1.19E-02	64.25	702.83	58.81	20.09
e^*_{KL}	5.97E-03	1.89E-04	5.78E-03	31.64	340.47	46.79	16.67
e_{Random}	4.70E-04	1.89E-04	2.81E-04	2.49	16.57	10.67	4.40

Table A3. Costs and various VoI metrics for risk-averse profile and the first eight sensors.

Risk averse profile considering sensors designs consisting of the first eight sensors

Designs	C_{savedLC} (in \$)	$C_{\text{investedLC}}$ (in \$)	EVoI_{LC} (in \$)	λ_{LC} (unitless)	$R_{\text{arithmetic}}$ (in %)	$R_{\text{geometric}}$ (in %)	$R_{\text{exponential}}$ (in %)
$e^*_{\text{EVoI}_{\text{LC}}}$	1.29E-02	3.77E-04	1.25E-02	34.13	368.09	48.03	17.03
$e^*_{\lambda_{\text{LC}}}$	1.11E-02	3.77E-04	1.07E-02	29.36	315.15	45.58	16.31
e^*_{KL}	9.42E-03	3.77E-04	9.05E-03	24.97	266.33	42.98	15.53
e_{Random}	3.97E-03	3.77E-04	3.59E-03	10.52	105.77	29.88	11.36

Table A4. Costs and various VoI metrics for risk-averse profile and the first sensor only.

Risk neutral profile considering sensors designs consisting of the first sensor only

Designs	C_{savedLC} (in \$)	$C_{\text{investedLC}}$ (in \$)	EVoI_{LC} (in \$)	λ_{LC} (unitless)	$R_{\text{arithmetic}}$ (in %)	$R_{\text{geometric}}$ (in %)	$R_{\text{exponential}}$ (in %)
$e^*_{\text{EVoI}_{\text{LC}}}$	1.22E-02	4.72E-05	1.21E-02	258.16	2857.36	85.35	26.80
$e^*_{\lambda_{\text{LC}}}$	1.55E-02	4.72E-05	1.54E-02	327.87	3631.94	90.34	27.95
e^*_{KL}	2.17E-03	4.72E-05	2.13E-03	46.09	501.04	53.06	18.48
e_{Random}	0	4.72E-05	−4.72E-05	0.00	−11.11	−100.00	−∞

For risk-neutral profile RP2

Table A5. Costs and various VoI metrics for risk-averse profile and the first four sensors.

Risk neutral profile considering sensors designs consisting of the first four sensors

Designs	$C_{savedLC}$ (in \$)	$C_{investedLC}$ (in \$)	$EVoI_{LC}$ (in \$)	λ_{LC} (unitless)	$R_{arithmetic}$ (in %)	$R_{geometric}$ (in %)	$R_{exponential}$ (in %)
$e^*_{EVoI_{LC}}$	1.50E-02	1.89E-04	1.48E-02	79.64	873.81	62.64	21.12
$e^*_{\lambda_{LC}}$	1.55E-02	1.89E-04	1.53E-02	82.18	902.04	63.21	21.28
e^*_{KL}	3.85E-03	1.89E-04	3.67E-03	20.42	215.80	39.82	14.56
e_{Random}	2.70E-04	1.89E-04	8.09E-05	1.43	4.77	4.05	1.72

Table A6. Costs and various VoI metrics for risk-averse profile and the first eight sensors.

Risk neutral profile considering sensors designs consisting of the first eight sensors

Designs	$C_{savedLC}$ (in \$)	$C_{investedLC}$ (in \$)	$EVoI_{LC}$ (in \$)	λ_{LC} (unitless)	$R_{arithmetic}$ (in %)	$R_{geometric}$ (in %)	$R_{exponential}$ (in %)
$e^*_{EVoI_{LC}}$	1.45E-02	3.77E-04	1.42E-02	38.52	416.88	50.03	17.62
$e^*_{\lambda_{LC}}$	1.50E-02	3.77E-04	1.46E-02	39.69	429.94	50.53	17.76
e^*_{KL}	8.32E-03	3.77E-04	7.94E-03	22.05	233.84	41.01	14.93
e_{Random}	0	3.77E-04	−3.77E-04	0.00	−11.11	−100.00	−∞

Table A7. Costs and various VoI metrics for risk-seeker profile and the first sensor only.

Risk seeker profile considering sensors designs consisting of the first sensor only

Designs	$C_{savedLC}$ (in \$)	$C_{investedLC}$ (in \$)	$EVoI_{LC}$ (in \$)	λ_{LC} (unitless)	$R_{arithmetic}$ (in %)	$R_{geometric}$ (in %)	$R_{exponential}$ (in %)
$e^*_{EVoI_{LC}}$	1.57E-02	4.72E-05	1.57E-02	332.72	3685.77	90.65	28.02
$e^*_{\lambda_{LC}}$	1.69E-02	4.72E-05	1.69E-02	358.46	3971.77	92.23	28.38
e^*_{KL}	1.30E-02	4.72E-05	1.29E-02	274.53	3039.19	86.62	27.10
e_{Random}	1.34E-04	4.72E-05	8.70E-05	2.85	20.50	12.32	5.05

For risk-seeker profile RP3

Table A8. Costs and various VoI metrics for risk-seeker profile and the first four sensors.

Risk seeker profile considering sensors designs consisting of the first four sensors

Designs	$C_{savedLC}$ (in \$)	$C_{investedLC}$ (in \$)	$EVoI_{LC}$ (in \$)	λ_{LC} (unitless)	$R_{arithmetic}$ (in %)	$R_{geometric}$ (in %)	$R_{exponential}$ (in %)
$e^*_{EVoI_{LC}}$	1.66E-02	1.89E-04	1.65E-02	88.17	968.60	64.49	21.61
$e^*_{\lambda_{LC}}$	1.55E-02	1.89E-04	1.53E-02	82.06	900.66	63.19	21.27
e^*_{KL}	1.65E-02	1.89E-04	1.63E-02	87.40	959.97	64.33	21.57
e_{Random}	1.88E-04	1.89E-04	−3.42E-07	1.00	−0.02	−0.02	−0.01

Table A9. Costs and various VoI metrics for risk-seeker profile and the first eight sensors.

Risk seeker profile considering sensors designs consisting of the first eight sensors

Designs	$C_{savedLC}$ (in $)	$C_{investedLC}$ (in $)	$EVoI_{LC}$ (in $)	λ_{LC} (unitless)	$R_{arithmetic}$ (in %)	$R_{geometric}$ (in %)	$R_{exponential}$ (in %)
$e^*_{EVoI_{LC}}$	1.54E-02	3.77E-04	1.50E-02	40.79	442.11	50.99	17.90
$e^*_{\lambda_{LC}}$	1.65E-02	3.77E-04	1.61E-02	43.75	475.03	52.17	18.23
e^*_{KL}	1.58E-02	3.77E-04	1.55E-02	41.95	454.97	51.46	18.03
e_{Random}	0	3.77E-04	−3.77E-04	0.00	−11.11	−100.00	−∞

Table A10. Costs and various VoI metrics for risk-averse profile and the second sensor only.

Risk-averse profile considering sensors designs consisting of the second sensor only

Designs	$C_{savedLC}$ (in $)	$C_{investedLC}$ (in $)	$EVoI_{LC}$ (in $)	λ_{LC} (unitless)	$R_{arithmetic}$ (in %)	$R_{geometric}$ (in %)	$R_{exponential}$ (in %)
$e^*_{EVoI_{LC}}$	1.15E-04	4.72E-05	6.83E-05	2.45	16.09	10.46	9.95
$e^*_{\lambda_{LC}}$	1.45E-04	4.72E-05	9.81E-05	3.08	23.10	13.31	12.49
e^*_{KL}	4.10E-03	4.72E-05	4.05E-03	86.94	954.86	64.24	49.61
e_{Random}	0	4.72E-05	−4.72E-05	0.00	−11.11	−100.00	−∞

Cost data considering sensors starting with the second sensor (excluding the first sensor)

For risk-averse profile RP1

Table A11. Costs and various VoI metrics for risk-averse profile and the second to fourth sensors.

Risk-averse profile considering sensors designs consisting of the second to fourth sensors

Designs	$C_{savedLC}$ (in $)	$C_{investedLC}$ (in $)	$EVoI_{LC}$ (in $)	λ_{LC} (unitless)	$R_{arithmetic}$ (in %)	$R_{geometric}$ (in %)	$R_{exponential}$ (in %)
$e^*_{EVoI_{LC}}$	1.30E-02	1.42E-04	1.29E-02	91.94	1010.40	65.26	50.23
$e^*_{\lambda_{LC}}$	0	1.42E-04	−1.42E-04	0.00	−11.11	−100.00	−∞
e^*_{KL}	4.42E-03	1.42E-04	4.28E-03	31.25	336.13	46.59	38.25
e_{Random}	1.23E-04	1.42E-04	−1.84E-05	0.87	−1.45	−1.54	−1.55

Table A12. Costs and various VoI metrics for risk-averse profile and the second to eighth sensors.

Risk-averse profile considering sensors designs consisting of the second to eighth sensors

Designs	$C_{savedLC}$ (in $)	$C_{investedLC}$ (in $)	$EVoI_{LC}$ (in $)	λ_{LC} (unitless)	$R_{arithmetic}$ (in %)	$R_{geometric}$ (in %)	$R_{exponential}$ (in %)
$e^*_{EVoI_{LC}}$	1.31E-02	3.30E-04	1.28E-02	39.63	429.24	50.51	40.88
$e^*_{\lambda_{LC}}$	1.56E-04	3.30E-04	−1.74E-04	0.47	−5.86	−8.00	−8.34
e^*_{KL}	8.11E-03	3.30E-04	7.78E-03	24.55	261.66	42.71	35.56
e_{Random}	0	3.30E-04	−3.30E-04	0.00	−11.11	−100.00	−∞

Table A13. Costs and various VoI metrics for risk-neutral profile and the second sensor only.

Risk-neutral profile considering sensors designs consisting of the second sensor only

Designs	C_{savedLC} (in \$)	$C_{\text{investedLC}}$ (in \$)	EVoI_{LC} (in \$)	λ_{LC} (unitless)	$R_{\text{arithmetic}}$ (in %)	$R_{\text{geometric}}$ (in %)	$R_{\text{exponential}}$ (in %)
$e^*_{\text{EVoI}_{\text{LC}}}$	1.37E-02	4.72E-05	1.36E-02	290.25	3213.86	87.78	63.01
$e^*_{\lambda_{\text{LC}}}$	0	4.72E-05	$-$4.72E-05	0.00	$-$11.11	$-$100.00	$-\infty$
e^*_{KL}	2.14E-03	4.72E-05	2.10E-03	45.42	493.61	52.81	42.40
e_{Random}	4.54E-04	4.72E-05	4.07E-04	9.62	95.81	28.60	25.16

For risk-neutral profile RP2

Table A14. Costs and various VoI metrics for risk-neutral profile and the second to fourth sensors.

Risk-neutral profile considering sensors designs consisting of the second to fourth sensors

Designs	C_{savedLC} (in \$)	$C_{\text{investedLC}}$ (in \$)	EVoI_{LC} (in \$)	λ_{LC} (unitless)	$R_{\text{arithmetic}}$ (in %)	$R_{\text{geometric}}$ (in %)	$R_{\text{exponential}}$ (in %)
$e^*_{\text{EVoI}_{\text{LC}}}$	1.40E-02	1.42E-04	1.38E-02	98.66	1085.06	66.56	51.02
$e^*_{\lambda_{\text{LC}}}$	3.57E-04	1.42E-04	2.16E-04	2.52	16.92	10.83	10.28
e^*_{KL}	3.06E-03	1.42E-04	2.92E-03	21.65	229.46	40.73	34.17
e_{Random}	0	1.42E-04	$-$1.42E-04	0.00	$-$11.11	$-$100.00	$-\infty$

Table A15. Costs and various VoI metrics for risk-neutral profile and the second to eighth sensors.

Risk-neutral profile considering sensors designs consisting of the second to eighth sensors

Designs	C_{savedLC} (in \$)	$C_{\text{investedLC}}$ (in \$)	EVoI_{LC} (in \$)	λ_{LC} (unitless)	$R_{\text{arithmetic}}$ (in %)	$R_{\text{geometric}}$ (in %)	$R_{\text{exponential}}$ (in %)
$e^*_{\text{EVoI}_{\text{LC}}}$	1.37E-02	3.30E-04	1.34E-02	41.56	450.61	51.30	41.41
$e^*_{\lambda_{\text{LC}}}$	0	3.30E-04	$-$3.30E-04	0.00	$-$11.11	$-$100.00	$-\infty$
e^*_{KL}	5.78E-03	3.30E-04	5.45E-03	17.51	183.45	37.45	31.81
e_{Random}	1.68E-03	3.30E-04	1.35E-03	5.08	45.31	19.79	18.05

Table A16. Costs and various VoI metrics for risk-seeker profile and the second sensor only.

Risk-seeker profile considering sensors designs consisting of the second sensor only

Designs	C_{savedLC} (in \$)	$C_{\text{investedLC}}$ (in \$)	EVoI_{LC} (in \$)	λ_{LC} (unitless)	$R_{\text{arithmetic}}$ (in %)	$R_{\text{geometric}}$ (in %)	$R_{\text{exponential}}$ (in %)
$e^*_{\text{EVoI}_{\text{LC}}}$	0.00E + 00	4.72E-05	$-$4.72E-05	0.00	$-$11.11	$-$100.00	#NUM!
$e^*_{\lambda_{\text{LC}}}$	1.27E-05	4.72E-05	$-$3.45E-05	0.27	$-$8.13	$-$13.59	$-$14.61
e^*_{KL}	1.89E-03	4.72E-05	1.85E-03	40.13	434.77	50.72	41.02
e_{Random}	7.55E-04	4.72E-05	7.08E-04	16.00	166.65	36.08	30.81

For risk-seeker profile RP3

Table A17. Costs and various VoI metrics for risk-seeker profile and the second to fourth sensors.

Risk-seeker profile considering sensors designs consisting of the second to fourth sensors

Designs	C_{savedLC} (in \$)	$C_{\text{investedLC}}$ (in \$)	EVoI_{LC} (in \$)	λ_{LC} (unitless)	$R_{\text{arithmetic}}$ (in %)	$R_{\text{geometric}}$ (in %)	$R_{\text{exponential}}$ (in %)
$e^*_{\text{EVoI}_{\text{LC}}}$	1.91E-03	1.42E-04	1.77E-03	13.47	138.56	33.50	28.89
$e^*_{\lambda_{\text{LC}}}$	0	1.42E-04	$-$1.42E-04	0.00	$-$11.11	$-$100.00	$-\infty$
e^*_{KL}	1.63E-02	1.42E-04	1.62E-02	115.46	1271.81	69.50	52.77
e_{Random}	1.39E-02	1.42E-04	1.37E-02	97.92	1076.86	66.42	50.93

Table A18. Costs and various VoI metrics for risk-seeker profile and the second to eighth sensors.

Risk-seeker profile considering sensors designs consisting of the second to eighth sensors

Designs	C_{savedLC} (in \$)	$C_{\text{investedLC}}$ (in \$)	EVoI_{LC} (in \$)	λ_{LC} (unitless)	$R_{\text{arithmetic}}$ (in %)	$R_{\text{geometric}}$ (in %)	$R_{\text{exponential}}$ (in %)
$e^*_{\text{EVoI}_{\text{LC}}}$	1.69E-03	3.30E-04	1.36E-03	5.12	45.75	19.89	18.14
$e^*_{\lambda_{\text{LC}}}$	0.00E+00	3.30E-04	$-$3.30E-04	0.00	$-$11.11	$-$100.00	$-\infty$
e^*_{KL}	1.59E-02	3.30E-04	1.55E-02	48.06	522.94	53.77	43.03
e_{Random}	1.40E-02	3.30E-04	1.36E-02	42.32	459.08	51.61	41.61